Accepted Manuscript

Kinetic models of swelling and thermal stability of silver/poly(vinyl alcohol)/chitosan/graphene hydrogels

Katarina Nešović[a], Ana Janković[a], Aleksandra Perić-Grujić[a], Maja Vukašinović-Sekulić[a], Tamara Radetić[a], Ljiljana Živković[b], Soo-Jin Park[c,***], Kyong Yop Rhee[d,**], Vesna Mišković-Stanković[a,d,*]

[a]*Faculty of Technology and Metallurgy, University of Belgrade, Karnegijeva 4, 11000 Belgrade, Serbia*

[b]*Vinča Institute of Nuclear Sciences, University of Belgrade, Mike Petrovića Alasa 12–14, Belgrade 11000, Serbia*

[c]*Department of Chemistry, Inha University, Incheon 402751, South Korea*

[d]*Department of Mechanical Engineering, Kyung Hee University, Yongin 17104, South Korea*

*Corresponding author. Tel: + 381 11 3303 687; fax: + 381 11 3370 387. E-mail address: vesna@tmf.bg.ac.rs (V. Mišković-Stanković).

**Co-corresponding author. Tel.: +82 31 201 2565; fax: +82 31 202 6693. E-mail address: rheeky@khu.ac.kr (K.Y. Rhee)

***Co-corresponding author. Tel: +82 32 876 7234; fax: +82 32 867 5604 E-mail address: sjpark@inha.ac.kr (S.-J. Park)

Graphical abstract:

1
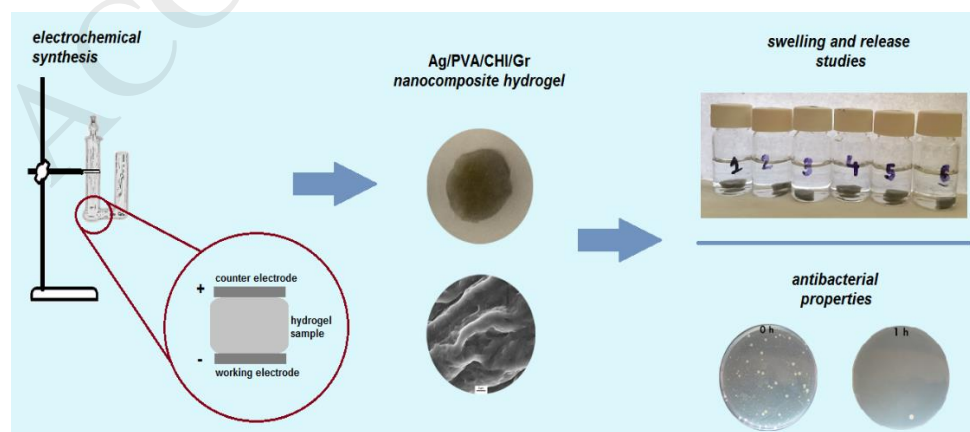
Highlights

- Electrochemical synthesis of silver nanoparticles in composite Ag/PVA/CHI/Gr hydrogel matrices
- Chitosan increased the thermal stability of Ag/PVA/CHI/Gr hydrogels
- Sorption diffusion models and silver release models were proved
- Synergistic effect of chitosan and silver nanoparticles on increased antibacterial activity

Abstract

Silver nanoparticles (AgNPs) were synthesized by *in situ* electrochemical reduction of Ag^+ ions in poly(vinyl alcohol)/chitosan/graphene (PVA/CHI/Gr) hydrogel matrices with different concentrations of chitosan. The physicochemical properties of nanocomposite hydrogels were investigated by ultraviolet-visible spectroscopy (UV-vis), dynamic light scattering (DLS), transmission electron microscopy (TEM), X-ray photoelectron spectroscopy (XPS), field-emission scanning electron microscopy (FE-SEM) and Fourier-transform infrared spectroscopy (FT-IR), thermal characteristics were determined by differential scanning calorimetry (DSC) and mechanical properties were measured by tensile test. The swelling studies were carried out in phosphate buffer to simulate natural physiological environment and data were fitted by several kinetic models to determine the diffusion mechanism and diffusion coefficients of the swelling medium through the hydrogel matrices. It was shown that the presence of silver nanoparticles increased the uptake capability and equilibrium swelling degree of the composite hydrogels. The antibacterial activity was confirmed against *Escherichia coli* and *Staphylococcus aureus*, while the hydrogels without AgNPs exhibited antibacterial properties due to the presence of chitosan. With the addition of AgNPs, the samples showed stronger activity and fast reduction in the number of colonies, confirming the synergistic effect of chitosan and AgNPs on the antibacterial activity.

1. Introduction

The next generation wound dressings need to conform to several criteria, such as biocompatibility and non-toxicity towards healthy cells and tissue, high exudate absorption capability, permeability for gasses such as oxygen and water vapor, the ability to keep the wound surroundings moist, sterility and barrier properties for the penetration of microorganisms, thermoregulatory properties and low adhesiveness, in order to prevent sticking to

the wound and possible new trauma during the dressing replacement [1,2]. Hydrogels, highly porous solid polymer matrices containing up to 90 % water, represent almost ideal wound dressing materials, which conform satisfactorily to all the above criteria. For that reason, many research works are lately dedicated to the investigation of hydrogel wound dressings with antibacterial properties, aimed to replace the traditional materials such as gauzes and bandages. Another reason for the use of hydrogel materials as wound dressings is the possibility of prolonged application, limiting the need for frequent dressing replacement and thereby minimizing the damage to the wound tissue. An important aspect is the choice of antibacterial agent, which should provide sterility of the wound dressing and prevent the adhesion of bacteria and biofilm formation during the initial 24 h of application [3]. Silver nanoparticles (AgNPs) are a broad-spectrum antimicrobial agent, exhibiting strong activity against many microorganisms, including Gram-positive and Gram-negative bacteria [4,5]. Moreover, silver nanoparticles can be efficiently immobilized in a polymer hydrogel to prevent their agglomeration and ensure long-term stability and time-dependent release at the wound site. Polymers such as poly(vinyl alcohol) (PVA) and chitosan (CHI) are known as good stabilizers for silver nanoparticles, and, moreover, CHI also possesses a certain ability to reduce the Ag^+ ions [6–11], acting at the same time as a reducing agent and a stabilizer for AgNPs.

Several recent research papers have investigated the possibility for preparation of PVA and CHI composite materials with AgNPs for biomedical applications [12–20]. Chitosan possesses good biocompatibility and intrinsic antibacterial activity due to its polycationic properties [21]. Hydrogels containing chitosan have been shown to exhibit antibacterial activity against *E. coli*, which is even more pronounced with the addition of AgNPs [12,14,15], indicating a possible synergistic effect of CHI and AgNPs. However, in the case of chitosan hydrogel blends with polyanionic polymers such as alginate (Alg), there was no antibacterial activity observed [16,22], due to the polyelectrolyte complex formation between NH_3^+ groups of chitosan and COO^- groups of Alg, leading to the decrease in number of positively charged groups that can interact with bacteria [17]. The antibacterial activity of chitosan films and nanocomposite hydrogels with different concentrations of AgNPs was investigated [9], and it was found that the films loaded with AgNPs possessed bactericidal properties against *E. coli* up to 20 days, whereas the neat chitosan films were bactericidal in the first 6 days, then bacteriostatic from day 6 to 18, and after 18 days they completely lost antibacterial properties. This behavior was explained by the different mechanisms of antibacterial activity of chitosan and AgNPs. The antibacterial activity of chitosan, as a polycationic polysaccharide, is achieved through binding to the negatively charged cytoplasmic membrane of bacterial cell and disrupting its normal functions. Moreover, bacterial cells tend to adsorb on the surface of

3

chitosan-based materials, leading to the inhibition of antibacterial properties at the point when the entire surface is covered with dead bacteria [9]. On the other hand, the AgNPs exhibit antibacterial properties through several different mechanisms, including the damage of cytoplasmic membrane, inhibition of ATP production, disruption of cell respiration and DNA replication [4,23–25]. It is also possible that AgNPs release a certain amount of silver ions, adding another dimension to their antibacterial activity and increasing and prolonging the bactericidal effect.

One drawback of CHI is its biodegradability in physiological environment [26], and its poor mechanical properties, which is why it is often blended with other polymers such as PVA enabling better mechanical properties and elasticity of the hydrogel wound dressing during prolonged use. Baring in mind the envisioned application of hydrogels as wound dressings with improved durability and with minimized frequency of replacement, the hydrogel material has to possess excellent structural integrity and good enough mechanical properties to prevent degradation of the dressing material during its use. For that reason, graphene is often incorporated in hydrogel matrices to improve their mechanical properties, as it has been shown to greatly improve tensile strength and elastic modulus of polymer-based materials [27–29].

The PVA/CHI hydrogel blends can be obtained by a simple freezing-thawing method [30–32], which allows to achieve a high degree of physical cross linking of the hydrogel without the necessity for the use of toxic cross linking agents, whereas the properties of thus obtained hydrogel can be fine-tuned by varying the freezing-thawing parameters, such as temperature, duration and number of cycles [32]. As already mentioned, the AgNPs can be obtained by reduction of Ag^+ with chitosan [9,11,15,33], which is a simple and green method for preparing nanocomposite hydrogels or films, but on the other hand, the synthesis can be time consuming as the time of reduction can last from 6 h up to 8-10 days [9,11,33], often at elevated temperatures [12]. It is therefore desirable to use some other, more efficient method for the synthesis of AgNPs. In our previous works, we have developed a fast, simple method of electrochemical synthesis of AgNPs *in situ* in the polymer matrix, which enables efficient synthesis of AgNPs and their direct immobilization inside the hydrogel [34–37]. Poly(vinyl alcohol) was chosen as the main structural component of the hydrogel as a biocompatible synthetic polymer with good elastic properties, and it was intended to provide structural integrity of the hydrogel matrix and to enable hydrogel cross linking *via* the freezing-thawing method [32]. Chitosan, as an antibacterial polysaccharide obtained from natural sources, was included as a biocompatible material which was already shown to possess antibacterial properties and the ability to promote and accelerate wound healing [38,39]. Both polymers also had an additional, but important role in stabilization of silver nanoparticles. The addition of chitosan in PVA

4

hydrogel contributed to the greater yield of the synthesized AgNPs as well as provided higher degree of stabilization of AgNPs *via* interactions with –OH and –NH$_2$ groups on CHI chain, as we have shown in our recently published paper [40]. Finally, graphene was used as a nano filler to improve mechanical properties of the hydrogels [41–43], especially bearing in mind the requirements for new wound dressing materials. Dressings should have a longer life span and prolonged applicability, in order to minimize the frequency of replacement of the wound dressing, which would alleviate the problem of possible wound tissue damage upon replacement [44,45]. It has been shown that well-dispersed graphene significantly improved tensile properties of both PVA and chitosan-based nanocomposites [46,47].

 The aim of this work was to investigate the effect of chitosan on swelling characteristics and thermal stability of produced nanocomposite silver/poly(vinyl alcohol)/chitosan/graphene hydrogels by *in situ* electrochemical synthesis of AgNPs in the PVA/CHI/Gr hydrogel matrix, aimed for biomedical applications as antibacterial wound dressings.

2. Materials and Methods

2.1 Material

The following reagents were used: PVA (fully hydrolyzed, molecular weight 70–100 kDa, Sigma Aldrich, USA), chitosan (medium molecular weight 190–310 kDa, deacetylation degree 75-85 %, Sigma Aldrich, USA), graphene (99.2 %, Graphene Supermarket, USA); glacial acetic acid (Beta Hem, Serbia); KNO$_3$ (Centrohem, Serbia); AgNO$_3$ (MP Hemija, Serbia); K$_2$HPO$_4$ (Kemika, Croatia) and KH$_2$PO$_4$ (Centrohem, Serbia); ultra-pure water Milli-Q (Millipore, USA).

2.2 Preparation of hydrogels and synthesis of silver nanoparticles

PVA colloid dispersions were obtained by dissolving PVA powder at 90^{0}C in distilled H$_2$O for 2-3 h under vigorous stirring, while chitosan was dissolved at 50 ^{0}C in 2 vol% CH$_3$COOH (aq). After cooling, the CHI colloid dispersion was slowly added into the PVA dispersion, which was constantly stirred on a magnetic stirrer. Graphene was then added, and the final dispersions were sonicated for 30 min. We prepared two colloid dispersions with 0.1 wt% and 0.5 wt% CHI, PVA (10 wt%) and Gr (0.01 wt%). Colloid PVA/CHI/Gr dispersions were cast onto Petri dishes (h = 5 mm) and subjected to 5 freeze-thaw cycles (one cycle: 16 h at – 18^{0}C, 8 h at +4^{0}C).

5

After the freezing-thawing cross linking, hydrogels were cut into small discs (h ~ 5 mm, d ~ 10-12 mm), and immersed in two different swelling solutions: 0.25 mM $AgNO_3$ and 3.9 mM $AgNO_3$, with 0.1 M KNO_3 added to improve the electrical conductivity of the swelling medium. AgNPs were obtained by *in situ* electrochemical reduction of Ag^+ in hydrogel matrices in a two-electrode (Pt working and counter electrodes) custom-made electrochemical cell [36]. DC power supply MA 8903 Electro-Phoresis (Iskra, Slovenia) was used to supply constant voltage (90 V). Between every two syntheses, Pt electrodes were rinsed in 1:1 (v/v) HNO_3 and washed with distilled H_2O.

Hydrogels with different chitosan content (0.1 and 0.5 wt%) prepared from different concentrations of $AgNO_3$ swelling solution (0.25 and 3.9 mM $AgNO_3$) were labeled as follows: PVA/0.1CHI/Gr (0.1 wt% chitosan), PVA/0.5CHI/Gr (0.5 wt% chitosan), 0.25Ag/PVA/0.1CHI/Gr (0.1 wt% chitosan, 0.25 mM swelling solution), 0.25Ag/PVA/0.5CHI/Gr (0.5 wt% chitosan, 0.25 mM swelling solution), 3.9Ag/PVA/0.1CHI/Gr (0.1 wt% chitosan, 3.9 mM swelling solution), 3.9Ag/PVA/0.5CHI/Gr (0.5 wt% chitosan, 3.9 mM swelling solution).

2.3 Ultraviolet-visible spectroscopy (UV-vis)

The UV-vis spectroscopy was performed on a UV-vis spectrophotometer (Mapada, China) in the wavelength range 300-700 nm. The samples were dissolved in hot dH_2O with the hydrogel/water ratio 1/5 by weight. The PVA/0.1CHI/Gr and PVA/0.5CHI/Gr hydrogels served as blank references. All spectra were recorded in triplicate and the reported results were the average of three samples.

2.4. X-ray photoelectron spectroscopy (XPS)

The XPS spectra of hydrogel samples were recorded on a photoelectron spectroscope K-Alpha System (Thermo Scientific, USA), operated with a Al Kα X-ray monochromator (1486.6 eV). The obtained C1s, O1s, N1s and Ag3d high-resolution spectra were fitted with Gaussian line shapes with a Shirley background correction. The element content quantification was carried out based on peak areas obtained by peak fitting, applying average matrix relative sensitivity factors for each element.

2.5. Transmission electron microscopy (TEM)

For TEM analysis, the 3.9Ag/PVA/0.1CHI/Gr and 3.9Ag/PVA/0.5CHI/Gr hydrogel samples were prepared by dissolving the hydrogel discs in hot dH_2O (1/20 ratio by weight). After dissolution, 15 μl of solutions were drop-casted on 400 mesh carbon-coated Cu grids and allowed to dry at ambient conditions for 24 h. TEM analysis was

carried out on Talos F200X G2 HRTEM instrument (FEI-Thermo Fisher Scientific, USA) at 200 keV

acceleration voltage. The micrograph analysis was performed using Gatan DigitalMicrograph software (Gatan,

USA).

2.6 Dynamic light scattering (DLS)

The hydrodynamic particle size and particle size distributions (PSD) of silver nanoparticles in

3.9Ag/PVA/0.1CHI/Gr and 3.9Ag/PVA/0.5CHI/Gr hydrogels were determined by DLS on a Zetasizer Nano ZS

instrument (Malvern, UK). The PVA/0.1CHI/Gr and PVA/0.5CHI/Gr hydrogels served as reference samples.

The instrument was equipped with a He–Ne laser (633 nm) and detection was performed with 173° scattering

angle. For DLS measurements, the hydrogel samples were dissolved in hot dH_2O in 1/5 ratio by weight (the

same as for UV-vis measurements). The Z-average hydrodynamic diameters (D_Z) and polydispersity indices

(PDI) were calculated as the average of 4 measurements, each based on 15 runs. The presented PSD data were

collected and averaged in the same manner.

2.7 Field-emission scanning electron microscopy (FE-SEM)

FE–SEM micrographs were obtained using LEO SUPRA 55 (Carl Zeiss AG, Germany). The FE-SEM

instrument was operated at acceleration voltage of 10 kV, equipped with an In-Lens detector in SE-BSE mode.

2.8 Fourier-transform infrared spectroscopy (FT-IR)

FT-IR spectroscopy was carried out in the 450–4000 cm^{-1} range, with a Perkin Elmer Spectrum One

spectrophotometer (Perkin Elmer Inc., USA). The samples were prepared for the analysis by drying for 48 h in a

dry sterilizer oven in order to remove the absorbed water from the hydrogels.

2.9 Tensile properties

The effect of graphene incorporation was investigated by testing the mechanical properties of the samples both

with and without graphene. For this purpose, the samples were prepared in film form, in order to achieve

standardized dimensions for tensile test experiments. The film samples were prepared as described in Section

2.2, and the only difference was that the colloid dispersions were cast on a flat plastic plate and dried until a

constant mass film was obtained (instead of freezing-thawing hydrogel preparation). The samples were prepared

both with and without the addition of graphene, namely PVA/0.1CHI, PVA/0.5CHI and PVA/0.5CHI/Gr.

Tensile tests were carried out on a Universal testing machine (self-production KHU, South Korea), with a 100 kgf load cell and with a loading rate of 0.5 mm/min.

2.10 Differential scanning calorimetry (DSC)

DSC evaluations of thermal stability of hydrogels in the temperature range of 20–600 ^{0}C (heating rate 20 ^{0}C/min) were carried out in TGA Q5000 IR/SDT Q600 (TA Instruments, USA). The scans were done under continuous N_2 flow (50 mL/min).

2.11 Sorption measurements

The gravimetric sorption experiments were done on PVA/0.1CHI/Gr, PVA/0.5CHI/Gr, 0.25Ag/PVA/0.1CHI/Gr, 0.25Ag/PVA/0.5CHI/Gr, 3.9Ag/PVA/0.1CHI/Gr and 3.9Ag/PVA/0.5CHI/Gr hydrogels. Hydrogels were dried at 37 ^{0}C until constant mass was reached, after which the pre-weighed dry xerogels were immersed in 10 ml phosphate buffer (PB), containing K_2HPO_4 and KH_2PO_4 (pH ~ 7.4) and stored in sterilizer oven at 37 ^{0}C. At different times (every 1 h for the first 10 h, and after that at 24, 27, 30, 48, 50, 52 and 72 h), gels were taken out of the solution and weighed (the excess liquid from the surface was removed by wiping with dry paper). The degree of swelling at time *t*, q_t, was determined using the following equation:

$$q_t = \frac{m_t - m_0}{m_0} \qquad (1)$$

Here, m_t is the mass of the hydrogel at time *t*, and m_0 is the initial mass of the dry xerogel. Equilibrium swelling degree, q_{eq}, was determined as the maximum swelling degree, i.e. the swelling degree the gel samples reached at equilibrium. All measurements were carried out in triplicate.

2.12 Atomic absorption spectroscopy

The release of antibacterial agent, silver nanoparticles, was monitored in PB for 28 days. Briefly, the experiment was performed as follows. The hydrogel disc samples were immersed in 10 ml of PB medium and kept at 37 ^{0}C in a sterilizer oven. The release medium was taken out at regular pre-set intervals (every 24 h for first 7 days, and then at day 9, 11, 14, 17, 22, 25 and 28) and replaced with fresh PB solution. The concentration of silver in thus obtained medium was determined using atomic absorption spectrophotometer PYU UNICAM (Koninklijke Philips, Netherlands). The measured concentrations were recalculated based on the hydrogel volume, and the amount of silver released at certain time was determined cumulatively. All results are reported as an average value for three samples.

2.13 Antibacterial test in suspension

Antibacterial activity of PVA/0.1CHI/Gr, PVA/0.5CHI/Gr, 0.25Ag/PVA/0.1CHI/Gr and 0.25Ag/PVA/0.5CHI/Gr hydrogels was evaluated against *Escherichia coli* ATCC 25922 and *Staphylococcus aureus* TL (culture collection Faculty of Technology and Metallurgy, University of Belgrade, Serbia). Hydrogel discs were cut into small cubes (approx. 2 mm x 2 mm), and then sterilized for 30 min under a UV-C lamp in a laminar air flow chamber. The antibacterial activity was evaluated by a test in suspension. A phosphate buffer (PB) medium was inoculated with fresh overnight (~ 18 h) bacteria cultures, with the initial number of cells in each suspension $\sim 10^5$-10^6 CFU ml^{-1}. Thus prepared suspensions were added into flasks containing hydrogel samples (~ 2 g), and a blank (bacteria in PB) with no samples was used as a control. The flasks with samples and control were incubated in water bath shaker (62 rpm) at 37 °C to ensure optimal thermal exchange. The number of bacterial cells was monitored at pre-determined time periods (15 min, 1 h, 3 h and 24 h) after inoculation. The aliquots were taken from the flasks and serially diluted. A 1.5 wt % nutrient agar (pre-cooled to ~55 ^{0}C), previously seeded with 100 μl of diluted culture medium, was gently stirred and poured over sterile Petri dishes. The number of viable cells was estimated and quantified (in CFU ml^{-1}) after 24 h incubation at 37 °C.

3. Results and discussion

3.1 Synthesis and characterization of hydrogels

The simple freezing/thawing method was applied in order to obtain physically cross linked hydrogels from PVA/CHI/Gr colloid dispersions. The cross linking of polymer chains and the formation of hydrogel is achieved *via* inter- and intramolecular hydrogen bonding between –OH and –NH$_2$ groups of PVA and CHI. The mechanism involves several steps during the freezing and thawing phases, including liquid-solid and liquid-liquid phase separation [30,31,36]. The number and duration of cycles, freezing/thawing temperatures greatly influence the properties of the obtained hydrogel network [48], such as porosity and gelation degree. The physical appearance of the hydrogel obtained by freezing-thawing method is presented in Fig. 1b. The gelation degree, W_g, of PVA/CHI/Gr hydrogels with different chitosan concentrations was determined as the ratio of xerogel weights before and after the extraction of non-cross linked phases from the gel, and we found that the PVA/0.5CHI/Gr hydrogel had $W_g = 94 \pm 0.2$ %, whereas the W_g of PVA/0.1CHI/Gr was 88 ± 9.3 % [40]. The higher W_g of PVA/0.5CHI/Gr hydrogel can be explained by the higher concentration of chitosan, containing more functional groups capable of hydrogen bonding, resulting in stronger cross linking of the hydrogels with 0.5 wt% CHI.

9

The freezing-thawing method for hydrogel cross linking provides highly effective, yet green and facile route for the preparation of the hydrogels, compared to conventional aldehyde-based chemical cross linking methods. In this work, we have shown that we were able to achieve very high gelation degrees with small percentage of the uncrosslinked polymer left in the matrix, which is advantageous over glutaraldehyde cross linking agent, widely used in similar-topic studies [12,14,15,20,49]. Glutaraldehyde is a toxic substance thus posing a potential health hazard, and has to be removed, extracted or washed out from the dressing [50], which could sometimes be tedious. On the other hand, freezing-thawing cross linking eliminates the need to use chemical cross linkers. Electrochemical synthesis of AgNPs is performed *in situ* in the hydrogel matrix, and the mechanism of their stabilization is well documented [36,37,51,52] and involves interactions with polymer chains and formation of coordination bonds with specific functional groups. The stabilization of AgNPs is achieved by the interactions with $-OH$ and $-NH_2$ functional groups on PVA and CHI chains, allowing coordination bonding and complex formation. Chitosan is known to possess strong chelating ability with metal cations [7,11], thus enabling even stronger immobilization of AgNPs than in PVA hydrogels alone [37].

The electrochemical method for the *in situ* synthesis of silver nanoparticles (AgNPs) in hydrogel matrices has been developed by our research group, and to the best of our knowledge has not been used by other researchers to date. The AgNPs have been synthesized in the hydrogel matrices of poly(vinyl pyrrolidone) [34], poly(vinyl alcohol) and poly(vinyl alcohol)/graphene [35,36]. This study further investigates the viability of AgNPs synthesis inside the poly(vinyl alcohol)/chitosan/graphene hydrogel matrices [40] and evaluates their potential for wound dressing applications. The advantage of *in situ* electrochemical AgNPs synthesis is that it is a green and facile method to obtain small-sized nanoparticles with excellent antibacterial activity [40]. The only chemicals used are silver nitrate and potassium nitrate in low concentrations in the swelling solutions, and the reduction of Ag^+ in the swollen hydrogel is achieved with either electrical current or hydrogen gas evolved on the cathode during the process. This allows facile incorporation of AgNPs inside the hydrogel matrix, and the duration of the synthesis is only 4 min at ambient conditions (room temperature, atmospheric pressure). Electrochemical method of in situ reduction of silver ions represents significant improvement over the other reported methods such as γ-irradiation [14,53,54], or chemical reduction [55,56], as it is much quicker and does not require neither specialized facilities, nor control of external conditions (e.g. temperature regulation), apart from setting the voltage parameters of the synthesis.

The first indication of the AgNP formation in the hydrogel is the yellowish color of the hydrogel after electrochemical synthesis (Fig. 1b). The successful incorporation of silver nanoparticles in PVA/CHI/Gr

10

hydrogels was confirmed by UV-visible spectroscopy (Fig. 1a), by the appearance of a narrow peak ~400 nm corresponding to the surface plasmon resonance (SPR) of AgNPs. Hydrogel with higher CHI content contained more AgNPs, as the absorbance of this peak increased in 3.9Ag/PVA/0.5CHI/Gr hydrogel, indicating a strong influence of chitosan on the yield of AgNPs electrochemical synthesis. Similar results were reported in previous work [40] on 0.25Ag/PVA/0.1CHI/Gr and 0.25Ag/PVA/0.5CHI/Gr hydrogel, where 0.25Ag/PVA/0.5CHI/Gr exhibited a higher absorbance of the SPR peak at ~400 nm and therefore contained higher amount of AgNPs. The position and width (specifically full width at half maximum, FWHM) of the SPR peaks indicated that the obtained nanoparticles were spherical and predominantly in the size range of 5-10 nm [57,58].

Fig. 1.

Table 1.

The presence of silver in metallic state was confirmed by XPS, as the Ag3d high-resolution spectrum contained two well-separated (~6 eV) spin-orbit splitting peaks at 368 eV and 374 eV, as shown in our previous study [40], which is a clear indication of the existence of metallic silver phase [59]. The atomic content of specific elements, determined by XPS, is presented in Table 1. All of the hydrogels contained the most carbon, followed by oxygen, whereas nitrogen content was fairly low due to the lower amounts of chitosan in the hydrogels than PVA. Hydrogels with 0.5 wt% CHI exhibited higher N content, compared to hydrogels with 0.1 wt% CHI. The Ag content in both 3.9Ag/PVA/0.1CHI/Gr and 3.9Ag/PVA/0.5CHI/Gr was similar (1.5 at% and 1.4 at%, respectively), contrary to the UV-visible spectroscopy results. However, XPS is a surface technique with a penetration depth of only several nanometers, so the element contents presented in Table 1 are indicative only of the amounts of different elements on the hydrogel surface. Since the XPS analysis showed similar amounts of Ag on the surface of both hydrogels, that might be an indication that the majority of AgNPs are embedded inside the 3.9Ag/PVA/0.5CHI/Gr hydrogel. That would further indicate the excess of chitosan provided good immobilization and dispersion of the nanoparticles. Such conclusion is further supported by SEM results and EDS analysis.

FE-SEM micrographs (Fig. 1c) indicated smaller and better dispersed AgNPs in the 3.9Ag/PVA/0.5CHI/Gr hydrogels than in 3.9Ag/PVA/0.1CHI/Gr. Better stabilization of AgNPs inside the matrix of the hydrogel with higher CHI content is a consequence of their stronger interactions with increasing number of functional $-NH_2$ and $-OH$ groups on the chitosan chain, which was further confirmed by FT-IR spectroscopy. The EDS analysis

from our previous work [40] showed higher Ag content in gels with more chitosan, i.e. 0.21 at% vs. 0.49 at% for 3.9Ag/PVA/0.1CHI/Gr and 3.9Ag/PVA/0.5CHI/Gr respectively.

The DLS method was employed in order to determine hydrodynamic size (diameter) and size distributions of silver nanoparticles incorporated in the studied hydrogels. The averaged intensity- and volume-weighted distributions are presented in Fig. 2a and 2e, for 3.9Ag/PVA/0.1CHI/Gr and 3.9Ag/PVA/0.5CHI/Gr respectively. In the case of both samples, the measurements revealed relatively narrow distributions with particle size in nm range. A rather small portion of large-sized fraction was also detected. The hydrogel with lower chitosan content (0.1 wt%) exhibited a monomodal distribution (Fig. 2a). Based on intensity data, the most abundant was the 9.97 nm-sized particle population (96.7 % share in the scattered light). The hydrogel with higher chitosan content (0.5 wt%) contained even smaller-sized AgNPs, which could be due to better stabilization of nanoparticles by interactions with functional groups on chitosan chains. Additionally, the PSD for 3.9Ag/PVA/0.5CHI/Gr hydrogel (Fig. 2e) was different in appearance compared to 3.9Ag/PVA/0.1CHI/Gr (Fig 2a), as the curves exhibited a bimodal distribution of particle sizes, with two peaks at 8.22 nm and 1.76 nm, respectively. Upon transformation to volume-weighted distribution, it was observed that the nanoparticles were predominantly (87.0 % by volume) in the smaller sized group (peak at ~1.57 nm), further corroborating the assumption that chitosan highly influenced the stabilization and growth of AgNPs in the hydrogel. The related Z-average hydrodynamic diameters (D_Z) of AgNPs were 8.06 ± 0.098 nm (PDI = 0.265 ± 0.032) for 3.9Ag/PVA/0.1CHI/Gr and 6.38 ± 0.12 nm (PDI = 0.387 ± 0.079) for 3.9Ag/PVA/0.5CHI/Gr. The polydispersity indices were relatively large, however, and larger in the case of 3.9Ag/PVA/0.5CHI/Gr (0.387 ± 0.079), suggesting that the nanoparticles incorporated in both hydrogel samples were not monodisperse. However, it was also likely that the large particles, present in both systems (Fig. 2), contributed to the overall polydispersity. In order to ascertain if the main peaks originated from AgNPs and not form other components in the systems, we also performed measurements for PVA/0.1CHI/Gr and PVA/0.5CHI/Gr hydrogels (data not shown), which revealed multimodal curves with larger particle sizes from 100 nm up to 1000 nm and with very high PDI~1, presumably originating from polymer chains or graphene particles in the dispersion.

TEM characterization confirmed the results of DLS analysis. The low-magnification micrographs (Fig. 2b and 2f) reveal the presence of some larger agglomerates, hundreds of nm in size, surrounded by numerous, finer AgNPs. Similarly to DLS results, characterization showed an almost bimodal distribution of AgNPs. Larger particles, ~10-20 nm in size, are heavily twinned and polycrystalline with faceted morphology. The facets tend to

12

be parallel to {111} planes like the particle in Fig. 2c that also exhibits a 6-fold twinning structure. Smaller AgNPs, ~5 nm in size, tend to be single crystals with cuboctahedral shape (Fig. 2d). In the case of 3.9Ag/PVA/0.5CHI/Gr hydrogel, there are many very small nanoparticles with sizes ~2 nm (Fig. 2h) surrounding some larger particles between 10-20 nm in size (Fig. 2g). The presence of very small AgNPs in 3.9Ag/PVA/0.5CHI/Gr hydrogel could be due to the contribution of higher chitosan content, as chitosan could influence both growth and stabilization of nanoparticles [6,61]. It is known that smaller-sized AgNPs possess much better antibacterial activity than larger nanoparticles [60], so the presence of AgNPs in a size range of <10 nm could prove invaluable for antibacterial applications of the prepared hydrogels.

That the observed nanoparticles are indeed AgNPs has been unquestionably confirmed by the FFT patterns typical for fcc crystal structure (inserts in Figs. 2d and 2h) and lattice fringe spacing of 0.24 nm and 0.20 nm corresponding to (111) and (200) crystal planes of fcc Ag.

Fig. 2.

These results indubitably confirmed the generation of AgNPs inside the polymer matrices of 3.9Ag/PVA/0.1CHI/Gr and 3.9Ag/PVA/0.1CHI/Gr, and their effective stabilization by PVA and CHI chains.

FT-IR spectra of PVA/0.1CHI/Gr and 3.9Ag/PVA/0.1CHI/Gr hydrogels (Fig. 3a) exhibited a broad, well defined absorption band ascribed to the stretching vibrations of hydrogen-bonded –OH groups positioned at 3295 cm^{-1} for PVA/0.1CHI/Gr and at 3294 cm^{-1} for 3.9Ag/PVA/0.1CHI/Gr, with a possible overlap of –NH$_2$ stretching from chitosan [62]. A slight red shift in the absorption maximum in the sample with silver suggested interactions of silver nanoparticles with –OH groups in the polymer. The red shift of this band is also prominent in Fig. 3b, with the –OH stretching band shifting from 3275 cm^{-1} for PVA/0.5CHI/Gr to 3274 cm^{-1} for 3.9Ag/PVA/0.5CHI/Gr. This indicates stronger interactions between AgNPs and chitosan. The –OH valence vibration band is also very sensitive to hydrogen bonding [63]; therefore, it is obvious that increases in CHI concentration led to the formation of stronger and more numerous inter- and intra-molecular hydrogen bonds, as evidenced by the significant shift of this band from 3295 cm^{-1} (PVA/0.1CHI/Gr) to 3275 cm^{-1} (PVA/0.5CHI/Gr).

Bands corresponding to C–O stretching vibrations in secondary alcohols (PVA) were located at 1087 cm^{-1} (PVA/0.1CHI/Gr), 1086 cm^{-1} (3.9A PVA/0.1CHI/Gr), 1088 cm^{-1} (PVA/0.5CHI/Gr) and 1080 cm^{-1} (3.9Ag/PVA/0.5CHI/Gr). The shift in the absorption maxima to lower wavenumbers in hydrogels containing

13

silver indicated interactions of AgNPs with PVA chains and the formation of complex bonds with –OH groups, leading to changes in C–O bond vibrations and IR absorption at lower wavenumbers. We suppose the blue shift in the absorption maximum with increased CHI concentration (comparing PVA/0.1CHI/Gr and PVA/0.5CHI/Gr) is a consequence of strong intermolecular hydrogen bonds between –OH groups of PVA and –OH and –NH$_2$ groups of chitosan, as discussed earlier.

Fig. 3

A sharp weak band originating from C–C symmetric stretching in PVA, is located at 1143 cm^{-1} (for both PVA/0.1CHI/Gr and PVA/0.5CHI/Gr), 1142 cm^{-1} (3.9A PVA/0.1CHI/Gr) and 1141 cm^{-1} (3.9AgPVA/0.5CHI/Gr). As this band's location and intensity are sensitive to polymer crystallinity [64], we assume that the presence of AgNPs influenced the crystalline structure of the PVA chain. Stretching of the carbonyl (C=O) bond of secondary amides (R–CO–NH–R') is present as a broad, but sharp band around 1650 cm^{-1} (the so called amide I absorption band) [63]. A slight shift of this band to higher wavenumbers was observed in the spectra of nanocomposite hydrogels with AgNPs (1652 cm^{-1} for 3.9Ag/PVA/0.1CHI/Gr and 1654 cm^{-1} for 3.9Ag/PVA/0.5CHI/Gr). Additionally, an increase in CHI content in the hydrogel increased the wavenumber as well as the intensity of the band. This occurs due to hydrogen bonding of acetamide groups on the chitosan chain with OH and NH$_2$ groups on PVA and CHI [65]. Bands at around 830 cm^{-1} correspond to out-of-plane wagging and twisting of the primary amino (–NH$_2$) group in the chitosan macromolecule. A significant increase in intensity and a slight red shift of this band in the FT-IR spectra of samples with silver nanoparticles also indicated AgNP-CHI complex formation, contributing to the stabilization of AgNPs in the silver-doped hydrogels.

3.2 Mechanical properties

The influence of graphene on the hydrogels mechanical properties was evaluated by tensile testing, and the obtained results are presented in Fig. 4 and Table 2. The stress-strain curves of reference PVA/0.1CHI and PVA/0.5CHI samples without graphene (Fig. 4) exhibited fairly similar behavior, whereas the PVA/0.5CHI/Gr exhibited much higher tensile yield, indicating improved mechanical properties with the addition of graphene. The quantitative tensile data, namely tensile yield strength (σ_R), yield elongation (ε_R), Young's elasticity modulus (E_J), ultimate strength (σ_U), ultimate elongation (ε_R), were calculated from stress strain curves and presented in Table 2. The PVA/0.5CHI/Gr sample exhibited much higher yield and ultimate strengths (78.0 MPa and 63.1 MPa, respectively), as well as higher elasticity modulus (121.7 MPa) compared to both PVA/0.1CHI and PVA/0.5CHI, confirming that the incorporation of graphene significantly improved hydrogels' tensile

strength and elasticity. On the other hand, the elongation at break for PVA/0.5CHI/Gr (23.2 %) was slightly lower than PVA/0.1CHI (28.1 %) and PVA/0.5CHI (38.0 %) indicating that graphene-containing gels and films could be slightly more brittle. Chitosan is known to possess poor mechanical properties [66], therefore it is no surprise that PVA/0.5CHI exhibited lower tensile strength, ultimate strength and elastic modulus, than PVA/0.1CHI (Table 2). Graphene has been shown to significantly improve tensile properties of chitosan-based composites, even in small quantities [67], which is also in agreement with our present results.

Fig. 4.

Table 2.

3.3 DSC

The DSC curves (Fig. 5) of all hydrogels revealed apparently endothermic events. The first event, depicted by a large endothermic peak with two maxima, was ascribed to the evaporation and loss of water in different states in the hydrogel. Water in a hydrogel can adopt different states due to different interactions and dipole orientations [68–70]. Freezable or free water inside the pores of the gel accounts for the largest proportion in the hydrogel, and it evaporates at lower temperatures. The bound or intermediate forms of water consist of dipoles polarized and oriented around charged and hydrogen-bonded groups and/or structured into a solvent cage around hydrophobic segments [69]. The first step of free water evaporation was observed at 74 °C for PVA/0.1CHI/Gr, 97 °C for 3.9Ag/PVA/0.1CHI/Gr, 88 °C for PVA/0.5CHI/Gr and at 80 °C for 3.9Ag/PVA/0.5CHI/Gr (Figs. 5a and 5b, respectively). The bound water evaporated in the range of approximately 130-160 °C, with DSC peaks positioned at 137 °C for PVA/0.1CHI/Gr, 156 °C for 3.9Ag/PVA/0.1CHI/Gr, 147 °C for PVA/0.5CHI/Gr and 150 °C for 3.9Ag/PVA/0.5CHI/Gr. The first observation is a change in the areas of the first two peaks with a change in chitosan content; namely, the area of the second peak increased in the hydrogels with 0.5 wt% CHI (Fig. 5b) compared to those with 0.1 wt% CHI (Fig. 5a). This means that the ratio of bound-to-free water is higher in hydrogels with higher chitosan content, which can be explained by the increase in the amount of polar hydrophilic groups (i.e. $-NH_2$, $-OH$) that are able to interact with water dipoles and cause orientation and ordering, subsequently lowering the free water content in favor of bound water [69]. This conclusion is also corroborated by the increase in evaporation temperatures for both peaks in PVA/0.5CHI/Gr (88 and 147 °C) in comparison to PVA/0.1CHI/Gr (74 and 137 °C). Some further changes can be observed in the DSC curves with the addition of AgNPs. Water evaporation occurred at higher temperatures for 3.9Ag/PVA/0.1CHI/Gr in comparison to PVA/0.1CHI/Gr, and the peaks exhibited larger area, indicating that the hydrogel with AgNPs

15

contained a higher amount of both bound and free water. This could be due to interactions of water dipoles with AgNPs, which result in a solvent cage around them as well as separation of macromolecule chains due to the incorporation of AgNPs. However, the peak areas are significantly lower for the 3.9Ag/PVA/0.5CHI/Gr as compared to the PVA/0.5CHI/Gr, and the peak of free water evaporation is much wider, with a maximum at lower temperature (80 °C as compared to 88 °C for PVA/0.5CHI/Gr). Neto et al. [71] hypothesized that the interactions of water dipoles with polar groups differ in strength. Specifically, the binding of water to amino groups in chitosan is weaker than binding to hydroxyl groups, and consequently this type of water bound to –NH_2 can be removed at lower temperatures. This may be an explanation for the higher bound water content in hydrogels with AgNPs, as AgNPs readily interact with –NH_2, which is an important factor in their stabilization and was explained previously. For that reason, –NH_2 groups are less available for interactions with water, and the dipoles are tightly bound (mainly to –OH groups), leading to an increase in bound water content. UV-vis (Section 3.1) showed that the hydrogel with higher chitosan content contained a higher amount of AgNPs than the hydrogel with lower chitosan content as a consequence of more interactions with both –NH_2 groups of CHI and –OH groups of CHI and PVA. This reduces the number of polar groups available for orientation and binding of water dipoles. Additionally, a high amount of AgNPs can contribute to the rigidity of a polymer network, thus reducing its water uptake capability. Those effects collectively lowered the amounts of both free and bound water in the 3.9Ag/PVA/0.5CHI/Gr hydrogel and resulted in a lower temperature of evaporation.

Second and third events in the DSC curves are related to the melting and onset of polymer matrix degradation, respectively. The peaks for these events were positioned at 220 °C and 272 °C for PVA/0.1CHI/Gr, 215 °C and 282 °C for 3.9Ag/PVA/0.1CHI/Gr, 218 °C and 276 °C for PVA/0.5CHI/Gr and at 219 °C and 293 °C for 3.9Ag/PVA/0.5CHI/Gr. The melting point (T_m) for pure PVA is usually found in the range of 202–218 °C, depending on the degree of crystallinity, cross linking density and preparation conditions [72–74], which is in good agreement with our results. The degradation of both PVA and CHI begins close to 300 °C, but their degradation behavior is different. Due to the much higher amount of PVA, the degradation peaks mainly represent the endothermic decomposition of PVA chains through scission reactions [75,76]. The increase in degradation temperature of PVA/0.5CHI/Gr (276 °C) compared to PVA/0.1CHI/Gr (272 °C) agrees with literature [46], and can be ascribed to the influence of chitosan. The thermal degradation of chitosan occurs *via* free radical-induced cross linking of the chains and the destruction of amino groups [68,77]. Depolymerization of the CHI chains continues up to 400 °C through dehydration, deamination and destruction of pyranose rings [77], also seen in Fig. 5 as slight peaks and shoulders at higher temperatures. The onset of degradation is clearly

16

shifted towards higher temperatures in both 3.9Ag/PVA/0.1CHI/Gr (282 °C) and 3.9Ag/PVA/0.5CHI/Gr (293 °C) hydrogels, indicating that the thermal stability is improved with the addition of AgNPs. A higher peak area for 3.9Ag/PVA/0.5CHI/Gr could be due to additional breakage of coordination bonds between AgNPs and polymer functional groups. Finally, at temperatures higher than 400 °C, the DSC curves exhibited mainly stable baselines, with few changes, indicating a thermally stable graphene-containing residue. At even higher temperatures, there is the possibility of some thermal oxidation of the residual graphene structure.

Fig. 5

3.4 Swelling

The sorption behavior of PVA/CHI/Gr and Ag/PVA/CHI/Gr hydrogels was monitored in PB solution at 37 °C. The dry xerogel and the swollen hydrogel at the end of the experiment are pictured in Fig. 1b. The swelling degree for PVA/0.5CHI/Gr was higher than for PVA/0.1CHI/Gr (Fig. 6a), indicating higher sorption ability of hydrogels with higher CHI content, which is in agreement with DSC investigations (Section 3.2), that proved the hydrogels with 0.5 wt% CHI exhibited higher capability for water uptake. This was also observed for hydrogels with AgNPs (Fig. 6b), and the presence of nanoparticles increased the maximum swelling degree of hydrogels, especially in the case of 3.9Ag/PVA/0.1CHI/Gr and 3.9Ag/PVA/0.5CHI/Gr. This was explained in DSC (Section 3.2), as the AgNPs could contribute to the increase of the bound water content *via* the orientation of water dipoles and formation of solvent cage around the nanoparticles. The equilibrium swelling degree, q_{eq}, as the maximum swelling degree reached at equilibrium, had the greater values for hydrogels with higher concentration of AgNPs and higher concentration of chitosan [40].

Fig. 6

The swelling of hydrophilic polymer gels is a complex process, especially in the case of polymers containing ionizable functional groups, such as amino groups on chitosan chain. The process of swelling is generally understood to take place *via* the formation of a moving front, with a sharp boundary between the solvated region (i.e. the swollen hydrogel phase) and the unsolvated polymer chains [78]. Initially, the concentration gradient of the swelling medium governs the swelling, as the dynamic sorption takes place by the mass transport of the solvent into the unsolvated region, moving the mentioned boundary inwards. Inside the swollen region, the disassociation of hydrogen bonds occurs, and just before the moving front, the presence of swelling medium causes the plasticizing of polymer chains, thus initiating the relaxation of polymer chains [78]. This complex

17

mechanism of gel swelling is thus governed by the three main processes – initial fast uptake of the medium through the pores of the gel, followed by longer, diffusion-controlled period of solvent penetration due to the concentration gradient inside the gel, and the last, usually short, phase where increase in swelling is achieved due to the polymer chain relaxation [79].

Generally, the experimental data can be fitted by several kinetic models in order to determine the sorption parameters, such as the diffusion coefficients of the solvent through the polymer network. Some of the most widely used sorption models include the early-time approximation (ETA), late-time approximation (LTA), and the Etters model [58,80,81], which are regarded to provide satisfactory description for the sorption processes.

The early-time approximation (ETA) is regarded to be valid for the initial 60 % of sorption, i.e. in the period where $q_t/q_{eq} < 0.6$. This model can be described by the equation (2), based on the Fick's second law of diffusion, where D_E is the diffusion coefficient of the swelling medium (subscript E denotes ETA model), t is the time at which the swelling degree q_t is reached and δ is the thickness of the sample. However, as shown by Ritger and Peppas [80], this equation is only satisfactory for the modeling of swelling of thin polymer films or slabs, i.e. the samples for which the so-called aspect ratio (the ratio of diameter and thickness, $2r/\delta$) is of the order >100. For the thick hydrogel discs with $2r/\delta \sim 1$, geometry of the sample must be taken into account, and the Fick's second law should be solved for the diffusion in both axial and radial direction [80]. Thus these authors proposed a modified ETA model, depicted by the equation (3), where r is the radius of the gel disc and other quantities have the previously defined meanings.

$$\frac{q_t}{q_{eq}} = 4 \left(\frac{D_E t}{\pi \, \delta^2}\right)^{1/2} \tag{2}$$

$$\frac{q_t}{q_{eq}} = 4\left(\frac{D_E \, t}{\pi \, r^2}\right)^{\frac{1}{2}} - \pi\left(\frac{D_E \, t}{\pi \, r^2}\right) - \frac{\pi}{3}\left(\frac{D_E \, t}{\pi \, r^2}\right)^{\frac{3}{2}} + 4\left(\frac{D_E \, t}{\pi \, \delta^2}\right)^{\frac{1}{2}} - \frac{2r}{\delta}\left[8\left(\frac{D_E \, t}{\pi \, r^2}\right) - 2\pi\left(\frac{D_E \, t}{\pi \, r^2}\right)^{3/2} - \right.$$

$$\left. \frac{2\pi}{3}\left(\frac{D_E \, t}{\pi \, r^2}\right)^2 \right] \tag{3}$$

In our case, the dimensions of as-prepared hydrogel discs were $2r \sim 10.5$ mm and $\delta \sim 5$ mm, whereas the dimensions of dried xerogels, which were used for swelling experiments, were $2r \sim 5$-6 mm and $\delta \sim 2$-3 mm. Thus we expected that the equation (3) (modified ETA) would provide a better model than the equation (2) (standard ETA). Indeed, the modified ETA model exhibited a much better correlation with our experimental data (Fig. 7), even extending the predictive capability of the model up to ~ 90 % of swelling, as suggested by Ritger

and Peppas [80]. As the modified ETA proved to be in better correlation with our experimental data than the standard ETA, further modeling was performed only using the equation (3).

Fig. 7

For the longer times, the sorption curves of PVA/0.1CHI/Gr and PVA/0.5CHI/Gr hydrogels were fitted to LTA (regarded to be valid for the last 40 % swelling ($0.6 < q_t/q_{eq} < 1.0$) and Etters models, described by the equations (4) and (5), respectively [81], where D_L is the diffusion coefficient of the swelling medium (subscript L denotes LTA model), D is the diffusion coefficient determined from the Etters model, a, b and k are the Etters constants, and other quantities have above defined meanings.

$$\frac{q_t}{q_{eq}} = 1 - \frac{8}{\pi^2} \exp\left(-\frac{D_L \pi^2 t}{\delta^2}\right) \qquad (4)$$

$$\frac{q_t}{q_{eq}} = 1 - \exp\left[-k\left(-\frac{D\,t}{\delta^2}\right)^a\right]^{1/b} \qquad (5)$$

Fig. 8 presents the ETA, LTA and Etters models for the PVA/0.1CHI/Gr and PVA/0.5CHI/Gr hydrogels. Etters model provided the best fit ($R^2 > 0.99$) for all samples over the entire time period up to 72 h. Similarly, the 0.25Ag/PVA/0.1CHI/Gr, 0.25Ag/PVA/0.5CHI/Gr, 3.9Ag/PVA/0.1CHI/Gr and 3.9Ag/PVA/0.5CHI/Gr hydrogels were also fitted by these three models, and only the Etters model, as the best fit, was presented here for clarity in the figures (Fig. 9).

Fig. 8

Fig. 9

The diffusion coefficients for all the samples, with and without the AgNPs, determined from the ETA (D_E), LTA (D_L) and Etters (D) models are presented in Table 3. All the diffusion coefficients of PB swelling medium through the hydrogel matrices were of the order of 10^{-8}. Generally, the D_E had the lowest and D_L the highest values, while D was always between these two values for all the samples. This means that the ETA model underestimates, while the LTA slightly overestimates the value of diffusion coefficient with regard to the Etters model, which provides the best fit for the entire time period.

The highest values of Etters diffusion coefficient, D, were observed for PVA/0.1CHI/Gr ($3.12 \times 10^{-8}\,cm^2\,s^{-1}$) and PVA/0.5CHI/Gr ($3.53 \times 10^{-8}\,cm^2\,s^{-1}$) and the lowest for 3.9Ag/PVA/0.1CHI/Gr ($0.940 \times 10^{-8}\,cm^2\,s^{-1}$) and

19

3.9Ag/PVA/0.5CHI/Gr (0.983×10^{-8} cm^2 s^{-1}), indicating that the hydrogels without the AgNPs exhibit the higher swelling rate and reach the equilibrium faster, whereas the hydrogels with AgNPs have slower swelling rate, but their equilibrium swelling degree is higher (273 ± 40 % and 261 ± 21 % for 3.9Ag/PVA/0.1CHI/Gr and 3.9Ag/PVA/0.5CHI/Gr, respectively, in comparison with 182 ± 33 % and 212 ± 14 % for PVA/0.1CHI/Gr and PVA/0.5CHI/Gr, respectively [40]).

Table 3

3.5 Silver release

The release of silver from the 3.9Ag/PVA/0.1CHI/Gr and 3.9Ag/PVA/0.5CHI/Gr hydrogel matrices was investigated over 28 days in phosphate buffer (PB) medium, and the amounts of released silver at time *t* was determined cumulatively as a sum of released silver up to that period. Thus obtained release profiles were fitted with kinetic models in order to examine the mechanism of silver release and to calculate the kinetic parameters. The first model used was Korsmeyer-Peppas model [82], described by equation (6), where $C_{\mathrm{Ag,t}}$ is the concentration of released silver at time *t*, $C_{\mathrm{Ag,in}}$ is the initial concentration of silver in the hydrogel and k_{KP} is the Korsmeyer-Peppas constant. This model is generally used to investigate the mechanism of mass transport dominating the release from hydrogel discs, and the value of exponent n indicates the governing mechanism, as for n < 0.5 the release follows Fick's law of diffusion, for n > 0.5 the release is achieved via non-Fickian, or anomalous diffusion, and for n = 1 the governing mechanism is Case II transport [82]. The second model is Makoid-Banakar model [83] represented by equation (7), where k_{MB}, n and C are parameters related to the constraint of the model which requires that the total dissolution of released substance must occur at a time when the Makoid-Banakar function approaches maximum value.

$$\frac{C_{\mathrm{Ag,t}}}{C_{\mathrm{Ag,in}}} = k_{\mathrm{KP}} \cdot t^{\mathrm{n}} \qquad\qquad (6)$$

$$\frac{C_{\mathrm{Ag,t}}}{C_{\mathrm{Ag,in}}} = k_{\mathrm{MB}} \cdot t^{\mathrm{n}} \cdot \exp(-\mathrm{c} \cdot t) \qquad\qquad (7)$$

The experimental profiles of silver release from 3.9Ag/PVA/0.1CHI/Gr and 3.9Ag/PVA/0.5CHI/Gr hydrogels and the corresponding models are presented in Fig. 10. Both profiles exhibited expected initial burst release during the first 3-5 days, followed by plateau of slower release over the longer period. This behavior is generally regarded as convenient for wound dressing applications, as the initial fast release of higher amount of silver is

desirable for the prevention of bacterial adhesion to the wound and biofilm formation, whereas slower release ensures sterility of the wound and the dressing during prolonged application [84]. Additionally, the hydrogels with higher chitosan content (3.9Ag/PVA/0.5CHI/Gr) exhibited much slower release and higher percent of retained silver after 28 days (43 ± 3.8 %), in comparison to 3.9Ag/PVA/0.1CHI/Gr (12 ± 0.5 %), indicating better stabilization of AgNPs in hydrogels with higher chitosan content. This is in agreement with the silver release results for 0.25Ag/PVA/0.1CHI/Gr and 0.25Ag/PVA/0.5CHI/Gr hydrogels [40], which retained 49.6% and 61.8% of initial concentration of silver in the hydrogel. The initial concentration of Ag in 3.9Ag/PVA/0.1CHI/Gr and 3.9Ag/PVA/0.5CHI/Gr hydrogels was 555.6 ± 10.1 mg dm^{-3} and 563.1 ± 6.7 mg dm^{-3}, respectively, indicating that the hydrogels with higher CHI content also contained higher amount of AgNPs, which is in agreement with the results of UV-vis spectroscopy (Section 3.1.).

The values of Korsmeyer-Peppas and Makoid-Banakar models parameters, calculated by fitting the experimental data, are presented in Table 4. The release of silver from hydrogel matrices is achieved *via* Fickian diffusion mechanism, as evidenced by the values of Korsmeyer-Peppas parameter n < 0.5. The Makoid-Banakar model provided slightly better fit for the experimental data, as shown by higher R^2 values. When the value of parameter C approaches 0, the Makoid-Banakar model becomes equal to Korsmeyer-Peppas. Obviously, the values of C for both 3.9Ag/PVA/0.1CHI/Gr (0.0063) and 3.9Ag/PVA/0.5CHI/Gr (0.0330) were low but not equal to zero, so the introduction of exponential parameter in the model, related to the dissolution of released silver in PB, evidently provides a better correlation with the experimental data. Additionally, the Makoid-Banakar parameter n was lower for 3.9Ag/PVA/0.1CHI/Gr (0.130) than for 3.9Ag/PVA/0.5CHI/Gr hydrogel (0.581), indicating faster release of silver from the hydrogel with lower chitosan content.

Fig. 10

The third model, used to describe the release behavior in the initial period and to calculate the diffusion coefficients of released silver through the polymer matrix, was early time approximation model (ETA), expressed by the equation (8) [40,80], where D_{Ag} is diffusion coefficient of silver ions through the hydrogel matrix, r and δ are the radius and the thickness of the hydrogel disc, respectively, and other quantities are previously defined. Similarly to ETA model for the sorption profiles, here we used a modified ETA model proposed by Ritger and Peppas [80], in order to account for the geometry of the thick hydrogel disc samples.

The experimental data and calculated ETA models are presented in Fig. 11, as the dependence of the released silver fraction, $c_{Ag,t}/c_{Ag,in}$ and square root of time, $t^{1/2}$. The calculated diffusion coefficients of silver through the hydrogel network, D_{Ag}, are listed in the Table 4. The D_{Ag} value for 3.9Ag/PVA/0.5CHI/Gr (0.723×10^{-8} cm^2 s^{-1})

was much lower in comparison to 3.9Ag/PVA/0.1CHI/Gr (8.41×10^{-8} cm^2 s^{-1}), corroborating the conclusion that

the release of silver is slower from the hydrogel with higher chitosan content, and the similar results were

obtained for 0.25Ag/PVA/0.5CHI/Gr (1.22×10^{-9} cm^2 s^{-1}) and 0.25Ag/PVA/0.1CHI/Gr (3.63×10^{-9} cm^2 s^{-1}) [40].

$$\frac{C_{Ag,t}}{C_{Ag,in}} = 4\left(\frac{D_{Ag}\,t}{\pi\,r^2}\right)^{\frac{1}{2}} - \pi\left(\frac{D_{Ag}\,t}{\pi\,r^2}\right) - \frac{\pi}{3}\left(\frac{D_{Ag}\,t}{\pi\,r^2}\right)^{\frac{3}{2}} + 4\left(\frac{D_{Ag}\,t}{\pi\,\delta^2}\right)^{\frac{1}{2}} - \frac{2r}{\delta}\left[8\left(\frac{D_{Ag}\,t}{\pi\,r^2}\right) - 2\pi\left(\frac{D_{Ag}\,t}{\pi\,r^2}\right)^{3/2} - \right.$$

$$\left. \frac{2\pi}{3}\left(\frac{D_{Ag}\,t}{\pi\,r^2}\right)^2 \right] \tag{8}$$

Fig. 11

Table 4

3.6 Antibacterial activity

Fig. 12 represents the quantification of surviving bacterial cells in the presence of PVA/0.1CHI/Gr,

PVA/0.5CHI/Gr, 0.25Ag/PVA/0.1CHI/Gr and 0.25Ag/PVA/0.5CHI/Gr hydrogels. The reasoning behind our

choice of the Ag concentrations for antibacterial measurements took into consideration the strong antibacterial

effect as well as the potential cytotoxicity of AgNPs which has to be avoided, if the hydrogels are to be used in

medical applications. A previous study conducted by our group [35], found that the optimal concentration of Ag

in the swelling solution was 0.25 mM, as the hydrogels prepared this way exhibited no cytotoxic effect towards a

live human cell line, while at the same time providing more than sufficient antibacterial activity. When designing

a wound dressing material, it is crucially important to strike a balance between the physical properties,

antibacterial action and non-toxicity, and this is precisely the reason why we have chosen hydrogels with lower

Ag content as best candidates for the intended purpose. Moreover, based on previously done disc-diffusion test

the addition of chitosan improved the antibacterial properties of 0.25Ag/PVA/0.1CHI/Gr and

0.25Ag/PVA/0.5CHI/Gr hydrogels [40] in comparison to Ag/PVA/Gr without chitosan. Therefore, the use of

lower AgNPs concentration was justified in order to avoid the possibility of cytotoxic effect. A visible reduction

of the cell number occurred even after 15 min of incubation, especially in the case of 0.25Ag/PVA/0.5CHI/Gr

sample. Hydrogels without AgNPs exhibited certain antibacterial activity, though their silver-incorporated

counterparts possessed comparably stronger activity. After 1 h, 0.25Ag/PVA/0.1CHI/Gr and

0.25Ag/PVA/0.5CHI/Gr hydrogels caused complete reduction of bacterial cells for both *S. aureus* and *E. coli*.

Against *S. aureus*, all the samples exhibited strong bactericidal activity even after 1 h incubation, however, the

effect of PVA/0.1CHI/Gr and PVA/0.5CHI/Gr against *E. coli* was much less pronounced. The number of *E. coli*

22

bacteria was progressively reduced, however, only after 24 h PVA/0.5CHI/Gr caused ~5 logarithmic units reduction. Towards the end of monitoring, PVA/0.1CHI/Gr lost its antibacterial effect against *E. coli*, as observed by the slow bacterial growth (Fig. 12b). Those results indicated that the hydrogels with higher CHI content possessed stronger antibacterial activity, and moreover, the 0.25Ag/PVA/0.5CHI/Gr hydrogels exhibited synergistic antibacterial effect of CHI and AgNPs. These results are in agreement with the conclusions of earlier studies [9,12,14,15], where the hydrogels and films exhibited enhanced antibacterial activity with the addition of silver nanoparticles. Furthermore, the silver release profiles (Section 3.4.) correlate well with the antibacterial activity kinetics, as the burst release effect in PB medium during the first 24 h is certain to have an influence on the stronger antibacterial activity of hydrogels with AgNPs. The release of AgNPs, and possibly the release of Ag^+ ions from AgNPs in the inoculated medium is likely the main mode of nanocomposite hydrogels activity [85].

Based on the results obtained for very strong antibacterial activity of 0.25Ag/PVA/0.1CHI/Gr and 0.25Ag/PVA/0.5CHI/Gr hydrogels, and considering the fact that they are non-cytotoxic towards both MRC-5 and L929 fibroblast cell lines, as proved in our previous study [40], it can be concluded that the obtained nanocomposite hydrogels are potentially good materials for topical wound dressing applications.

Fig. 12

4. Conclusions

In this paper, the electrochemical *in situ* synthesis of silver nanoparticles was investigated in composite poly(vinyl alcohol)/chitosan/graphene hydrogels, to obtain nanocomposite polymer-based materials for wound dressing applications. The effect of chitosan on physicochemical, biological, sorption and silver release properties was investigated, and it was found that hydrogel with higher CHI content contained higher amount of AgNPs. The increase in chitosan content improved the sorption ability and water uptake capability, as shown by sorption measurements and DSC. It was shown that the addition of graphene significantly improved mechanical properties and tensile strength. The DLS measurements indicated a small size of the hydrodynamic diameters of AgNPs, which decreased with higher chitosan content in the hydrogel, and those results were in good agreement with TEM, which proved the presence of small-sized AgNPs with smaller diameters in hydrogels with higher CHI content. The hydrogels with 0.5 wt% CHI exhibited slower release profiles and retained higher percentage of initial silver concentration, in comparison to 0.1 wt% CHI samples, as determined by silver release measurements. This is a consequence of AgNPs stabilization inside the hydrogel matrix with higher CHI content, i.e. stronger binding of the silver nanoparticles to free –NH$_2$ and –OH groups on chitosan chain, as shown by FT-IR spectroscopy. The initial burst of silver release, followed by a plateau over longer time periods was deemed convenient for wound dressing applications. The antibacterial activity of the hydrogels was assessed using test in suspension, and all investigated hydrogel samples exhibited strong antibacterial effect, especially 0.25Ag/PVA/0.5CHI/Gr hydrogels, where synergistic effect of CHI and AgNPs was evident against both *S. aureus* and *E. coli*. To summarize, the obtained silver/poly(vinyl alcohol)/chitosan/graphene hydrogels exhibited desirable sorption, silver release and antibacterial properties, and can be regarded as good candidates for wound dressing materials applications.

Declarations of interest: none.

References

[1]   M. Naseri-Nosar, Z.M. Ziora, Carbohydr. Polym. 189 (2018) 379–98. 10.1016/j.carbpol.2018.02.003.

[2]   E. Caló, V. V. Khutoryanskiy, Eur. Polym. J. 65 (2015) 252–67. 10.1016/j.eurpolymj.2014.11.024.

[3]   S.L. Percival, P. Bowler, E.J. Woods, Wound Repair Regen. 16(1) (2008) 52–7. 10.1111/j.1524-475X.2007.00350.x.

[4]   J.S. Kim, E. Kuk, K.N. Yu, J.H. Kim, S.J. Park, H.J. Lee, S.H. Kim, Y.K. Park, Y.H. Park, C.Y. Hwang, Y.K. Kim, Y.S. Lee, D.H. Jeong, M.H. Cho, Nanomed-Nanotechnol. 3(1) (2007) 95–101. 10.1016/j.nano.2006.12.001.

[5]   W.R. Li, X.B. Xie, Q.S. Shi, H.Y. Zeng, Y.S. Ou-Yang, Y. Ben Chen, Appl. Microbiol. Biotechnol. 85(4) (2010) 1115–22. 10.1007/s00253-009-2159-5.

[6]   H. Huang, Q. Yuan, X. Yang, Colloid Surface B. 39(1–2) (2004) 31–7. 10.1016/j.colsurfb.2004.08.014.

[7]   Y.-K. Twu, Y.-W. Chen, C.-M. Shih, Powder Technol. 185(3) (2008) 251–7. 10.1016/j.powtec.2007.10.025.

[8]   D. Wei, W. Qian, Colloid Surface B. 62(1) (2008) 136–42. 10.1016/j.colsurfb.2007.09.030.

[9]   D. Wei, W. Sun, W. Qian, Y. Ye, X. Ma, Carbohydr. Res. 344(17) (2009) 2375–82. 10.1016/j.carres.2009.09.001.

[10]   A. Regiel, S. Irusta, A. Kyzioł, M. Arruebo, J. Santamaria, Nanotechnology 24(1) (2013) 015101. 10.1088/0957-4484/24/1/015101.

[11]   M. Kozicki, M. Kołodziejczyk, M. Szynkowska, A. Pawlaczyk, E. Lešniewska, A. Matusiak, A. Adamus, A. Karolczak, Carbohydr. Polym. 140 (2016) 74–87. 10.1016/j.carbpol.2015.12.017.

[12]   A.M. Abdelgawad, S.M. Hudson, O.J. Rojas, Carbohydr. Polym. 100 (2014) 166–78. 10.1016/j.carbpol.2012.12.043.

[13]   T.T.T. Nguyen, B. Tae, J.S. Park, J. Mater. Sci. 46(20) (2011) 6528–37. 10.1007/s10853-011-5599-0.

[14]   A.M. Elbarbary, N.M. El-Sawy, Polym. Bull. 74(1) (2017) 195–212. 10.1007/s00289-016-1708-1.

[15]   A.T. Hang, B. Tae, J.S. Park, Carbohydr. Polym. 82(2) (2010) 472–9. 10.1016/j.carbpol.2010.05.016.

[16]   T. Khampieng, S. Wongkittithavorn, S. Chaiarwut, P. Ekabutr, P. Pavasant, P. Supaphol, J. Drug Deliv. Sci. Technol. 44(December 2017) (2018) 91–100. 10.1016/j.jddst.2017.12.005.

[17]   J. Venkatesan, J.-Y. Lee, D.S. Kang, S. Anil, S.-K. Kim, M.S. Shim, D.G. Kim, Int. J. Biol. Macromol. 98 (2017) 515–25. 10.1016/j.ijbiomac.2017.01.120.

[18]   M.R. Guascito, D. Chirizzi, R.A. Picca, E. Mazzotta, C. Malitesta, Mater. Sci. Eng. C 31(3) (2011) 606–11. 10.1016/j.msec.2010.11.022.

[19]   F.M. Reicha, A. Sarhan, M.I. Abdel-Hamid, I.M. El-Sherbiny, Carbohydr. Polym. 89(1) (2012) 236–44. 10.1016/j.carbpol.2012.03.002.

[20]   W. Yang, E. Fortunati, F. Bertoglio, J.S. Owczarek, G. Bruni, M. Kozanecki, J.M. Kenny, L. Torre, L. Visai, D. Puglia, Carbohydr. Polym. 181(March 2017) (2018) 275–84. 10.1016/j.carbpol.2017.10.084.

[21]   E.I. Rabea, M.E.-T. Badawy, C. V. Stevens, G. Smagghe, W. Steurbaut, Biomacromolecules 4(6) (2003) 1457–65. 10.1021/bm034130m.

[22]   D. Li, J. Diao, J. Zhang, J. Liu, J. Nanosci. Nanotechnol. 11(6) (2011) 4733–8. 10.1166/jnn.2011.4179.

[23]   M. Rai, A. Yadav, A. Gade, Biotechnol. Adv. 27(1) (2009) 76–83. 10.1016/j.biotechadv.2008.09.002.

[24]   Q.L. Feng, J. Wu, G.Q. Chen, F.Z. Cui, T.N. Kim, J.O. Kim, J. Biomed. Mater. Res. 52(4) (2000) 662–8. 10.1002/1097-4636(20001215)52:4<662::AID-JBM10>3.0.CO;2-3.

[25]   N. Duran, M. Duran, M.B. de Jesus, A.B. Seabra, W.J. Favaro, G. Nakazato, Nanomed-Nanotechnol. 12(3) (2016) 789–99. 10.1016/j.nano.2015.11.016.

[26]   S. Deepthi, J. Venkatesan, S.-K. Kim, J.D. Bumgardner, R. Jayakumar, Int. J. Biol. Macromol. 93 (2016) 1338–53. 10.1016/j.ijbiomac.2016.03.041.

[27]   J. Liang, Y. Huang, L. Zhang, Y. Wang, Y. Ma, T. Cuo, Y. Chen, Adv. Funct. Mater. 19(14) (2009) 2297–302. 10.1002/adfm.200801776.

[28] S. Shang, L. Gan, C.W.M. Yuen, S.X. Jiang, N.M. Luo, Compos. Part A Appl. Sci. Manuf. 68 (2015) 149–54. 10.1016/j.compositesa.2014.10.011.

[29] J. Wang, X. Wang, C. Xu, M. Zhang, X. Shang, Polym. Int. 60(5) (2011) 816–22. 10.1002/pi.3025.

[30] N.A. Peppas, S.R. Stauffer, J. Control. Release 16(3) (1991) 305–10. 10.1016/0168-3659(91)90007-Z.

[31] F. Yokoyama, I. Masada, K. Shimamura, T. Ikawa, K. Monobe, Colloid Polym Sci 264(7) (1986) 595–601.

[32] S.R. Stauffer, N.A. Peppas, Polymer. 33(18) (1992) 3932–6.

[33] H.V. Tran, L.D. Tran, C.T. Ba, H.D. Vu, T.N. Nguyen, D.G. Pham, P.X. Nguyen, Colloid Surface A. 360(1–3) (2010) 32–40. 10.1016/j.colsurfa.2010.02.007.

[34] Z. Jovanovic, A. Radosavljević, J. Stojkovska, B. Nikolić, B. Obradović, Z. Kacarevic-Popovic, V. Miskovic-Stankovic, Polym. Compos. 35(2) (2014) 217–26. 10.1002/pc.22653.

[35] M.M. Abudabbus, I. Jevremović, A. Janković, A. Perić-Grujić, I. Matić, M. Vukašinović-Sekulić, D. Hui, K.Y. Rhee, V. Mišković-Stanković, Compos. Part B Eng. 104 (2016) 26–34. 10.1016/j.compositesb.2016.08.024.

[36] M.M. Abudabbus, I. Jevremović, K. Nešović, A. Perić-Grujić, K.Y.K.Y. Rhee, V. Mišković-Stanković, Compos. Part B Eng. 140 (2018) 99–107. 10.1016/j.compositesb.2017.12.017.

[37] K. Nešović, V. Kojić, K.Y. Rhee, V. Mišković-Stanković, Corrosion 73(12) (2017) 1437–47. 10.5006/2507.

[38] N. Bhattarai, J. Gunn, M. Zhang, Adv. Drug Deliv. Rev. 62(1) (2010) 83–99. 10.1016/j.addr.2009.07.019.

[39] A. Kumar, M. Jaiswal, J. Appl. Polym. Sci. 133(14) (2016) 1–14. 10.1002/app.43260.

[40] K. Nešović, A. Janković, V. Kojić, M. Vukašinović-Sekulić, A. Perić-Grujić, K.Y.K.Y. Rhee, V. Mišković-Stanković, Compos. Part B Eng. 154 (2018) 175–85. 10.1016/j.compositesb.2018.08.005.

[41] R. Surudžić, A. Janković, M. Mitrić, I. Matić, Z.D. Juranić, L. Živković, V. Mišković-Stanković, K.Y. Rhee, S.J. Park, D. Hui, J. Ind. Eng. Chem. 34 (2016) 250–7. 10.1016/j.jiec.2015.11.016.

[42] G. Mittal, K.Y. Rhee, S.J. Park, D. Hui, Compos. Part B Eng. 114 (2017) 348–55. 10.1016/j.compositesb.2017.02.018.

[43] V. Dhand, K.Y. Rhee, H.J. Kim, D.H. Jung, J. Nanomater. 2013 (2013) 1–14. 10.1155/2013/763953.

[44] J. Koehler, F.P. Brandl, A.M. Goepferich, Eur. Polym. J. 100 (2018) 1–11. 10.1016/j.eurpolymj.2017.12.046.

[45] D. Eisenbud, H. Hunter, L. Kessler, K. Zulkowski, Ostomy-Wound Manag. 49(10) (2003) 52–7.

[46] J. Guo, L. Ren, R. Wang, C. Zhang, Y. Yang, T. Liu, Compos. Part B Eng. 42(8) (2011) 2130–5. 10.1016/j.compositesb.2011.05.008.

[47] J.H. Lee, J. Marroquin, K.Y. Rhee, S.J. Park, D. Hui, Compos. Part B Eng. 45(1) (2013) 682–7. 10.1016/j.compositesb.2012.05.011.

[48] T. Fukumori, T. Nakaoki, J. Appl. Polym. Sci. 131(15) (2014) 1–8. 10.1002/app.40578.

[49] S. Agnihotri, S. Mukherji, S. Mukherji, Appl.Nanosci. 2(3) (2012) 179–88. 10.1007/s13204-012-0080-1.

[50] B. Hoffmann, D. Seitz, A. Mencke, A. Kokott, G. Ziegler, J. Mater. Sci. Mater. Med. 20(7) (2009) 1495–503. 10.1007/s10856-009-3707-3.

[51] B. Yin, H. Ma, S. Wang, S. Chen, J. Phys. Chem. B 107(34) (2003) 8898–904. 10.1021/jp0349031.

[52] L. Kvítek, A. Panácek, J. Soukupova, M. Kolar, R. Vecerova, R. Prucek, M. Holecova, R. Zboril, J. Phys. Chem. 112(15) (2008) 5825–34. 10.1021/jp711616v.

[53] K.A.A. Juby, C. Dwivedi, M. Kumar, S. Kota, H.S.S. Misra, P.N.N. Bajaj, Carbohydr. Polym. 89(3) (2012) 906–13. 10.1016/j.carbpol.2012.04.033.

[54] N. Eghbalifam, M. Frounchi, S. Dadbin, Int. J. Biol. Macromol. 80 (2015) 170–6. 10.1016/j.ijbiomac.2015.06.042.

[55] Y. Murali Mohan, K. Lee, T. Premkumar, K.E. Geckeler, Polymer. 48(1) (2007) 158–64. 10.1016/j.polymer.2006.10.045.

[56] K. Vimala, K. Samba Sivudu, Y. Murali Mohan, B. Sreedhar, K. Mohana Raju, Carbohydr. Polym. 75(3)

(2009) 463–71. 10.1016/j.carbpol.2008.08.009.

[57]   A. Slistan-Grijalva, R. Herrera-Urbina, J.F. Rivas-Silva, M.. Avalos-Borja, F.F. Castillon-Barraza, A. Posada-Amarillas, Phys. E 25 (2005) 438–48. 10.1016/j.physe.2004.07.010.

[58]   J. Spasojević, A. Radosavljević, J. Krstić, D. Jovanović, V. Spasojević, M. Kalagasidis-Krušić, Z. Kačarević-Popović, Eur. Polym. J. 69 (2015) 168–85. 10.1016/j.eurpolymj.2015.06.008.

[59]   A.C. Joshi, G.B. Markad, S.K. Haram, Electrochim. Acta 161 (2015) 108–14. 10.1016/j.electacta.2015.02.077.

[60]   G.A. Martinez-Castanon, N. Niño-Martínez, F. Martínez-Gutierrez, J.R. Martínez-Mendoza, F. Ruiz, J. Nanoparticle Res. 10(8) (2008) 1343–8. 10.1007/s11051-008-9428-6.

[61]   H. Huang, X. Yang, Biomacromolecules 5(6) (2004) 2340–6. 10.1021/bm0497116.

[62]   P. Sharma, G. Mathur, S.R. Dhakate, S. Chand, N. Goswami, S.K. Sharma, A. Mathur, Carbohydr. Polym. 137 (2016) 576–83. 10.1016/j.carbpol.2015.10.096.

[63]   D. Mayo, F. Miller, R. Hannah, Course Notes On The Interpretation Of Infrared And Raman Spectra, John Wiley and Sons Ltd, 2003.

[64]   M. Miya, R. Iwamoto, S. Mima, J. Polym. Sci. Polym. Phys. Ed. 22(6) (1984) 1149–51. 10.1002/pol.1984.180220615.

[65]   S.J. Lee, Y. M.; Kim, S. H.; Kim, Polymer. 37(26) (1996) 5897–905. 10.1016/S0032-3861(96)00449-1.

[66]   S.F. Wang, L. Shen, W. De Zhang, Y.J. Tong, Biomacromolecules 6(6) (2005) 3067–72. 10.1021/bm050378v.

[67]   Z. Ge, Z. Jin, H. Fan, K. Zhao, L. Wang, Z. Shi, N. Li, Biomacromolecules 11(9) (2010) 2345–51. 10.1021/bm100470q.

[68]   M. Koosha, H. Mirzadeh, J. Biomed. Mater. Res. - Part A 103(9) (2015) 3081–93. 10.1002/jbm.a.35443.

[69]   T. Wang, S. Gunasekaran, J. Appl. Polym. Sci. 101(5) (2006) 3227–32. 10.1002/app.23526.

[70]   M. Mucha, A. Pawlak, Thermochim. Acta 427(1–2) (2005) 69–76. 10.1016/j.tca.2004.08.014.

[71]   C.G.T. Neto, J.A. Giacometti, A.E. Job, F.C. Ferreira, J.L.C. Fonseca, M.R. Pereira, Carbohydr. Polym. 62(2) (2005) 97–103. 10.1016/j.carbpol.2005.02.022.

[72]   H. Feng, Z. Feng, L. Shen, Polymer. 34(12) (1993) 2516–9. 10.1016/0032-3861(93)90581-T.

[73]   N.A. Peppas, E.W. Merrill, J. Appl. Polym. Sci. 20(6) (1976) 1457–65. 10.1002/app.1976.070200604.

[74]   S.R. Sudhamani, M.S. Prasad, K. Udaya Sankar, Food Hydrocoll. 17(3) (2003) 245–50. 10.1016/S0268-005X(02)00057-7.

[75]   S. Tanpichai, K. Oksman, Compos. Part A Appl. Sci. Manuf. 88 (2016) 226–33. 10.1016/j.compositesa.2016.06.002.

[76]   Q. An, C. Beh, H. Xiao, J. Appl. Polym. Sci. 131(1) (2014) 1–9. 10.1002/app.39720.

[77]   J. Zawadzki, H. Kaczmarek, Carbohydr. Polym. 80(2) (2010) 395–401. 10.1016/j.carbpol.2009.11.037.

[78]   K. De Yao, T. Peng, H.B. Feng, Y.Y. He, J. Polym. Sci. Part A Polym. Chem. 32(7) (1994) 1213–23. 10.1002/pola.1994.080320702.

[79]   X. Yang, Q. Liu, X. Chen, F. Yu, Z. Zhu, Carbohydr. Polym. 73(3) (2008) 401–8. 10.1016/j.carbpol.2007.12.008.

[80]   P.L. Ritger, N.A. Peppas, J. Control. Release 5(1) (1987) 23–36. 10.1016/0168-3659(87)90034-4.

[81]   M.P. Mullarney, T.A.P. Seery, R.A. Weiss, Polymer. 47(11) (2006) 3845–55. 10.1016/j.polymer.2006.03.096.

[82]   R.W. Korsmeyer, R. Gurny, E. Doelker, P. Buri, N.A. Peppas, Int. J. Pharm. 15(1) (1983) 25–35. 10.1016/0378-5173(83)90064-9.

[83]   J. Pais, J. Online Math. Its Appl. 1(2) (2001).

[84]   Ž. Jovanović, A. Radosavljević, Z. Kačarević-Popović, J. Stojkovska, A. Perić-Grujić, M. Ristić, I.Z. Matić, Z.D. Juranić, B. Obradovic, V. Mišković-Stankovic, Colloid Surface B. 105 (2013) 230–5. 10.1016/j.colsurfb.2012.12.055.

[85]   J.R. Morones, J.L. Elechiguerra, A. Camacho, K. Holt, J.B. Kouri, J.T. Ram, M.J. Yacaman, Nanotech

(16) (2005) 2346–53. 10.1088/0957-4484/16/10/059.

FIGURE CAPTIONS

Fig. 1. a) UV-vis spectra, b) representative photographs of hydrogels (I – hydrogel before AgNP synthesis, II – hydrogel with incorporated AgNPs, III – xerogel before sorption experiments, IV – swollen hydrogel after the sorption experiments) and c) FE-SEM micrographs of 3.9Ag/PVA/0.1CHI/Gr and 3.9Ag/PVA/0.5CHI/Gr hydrogels.
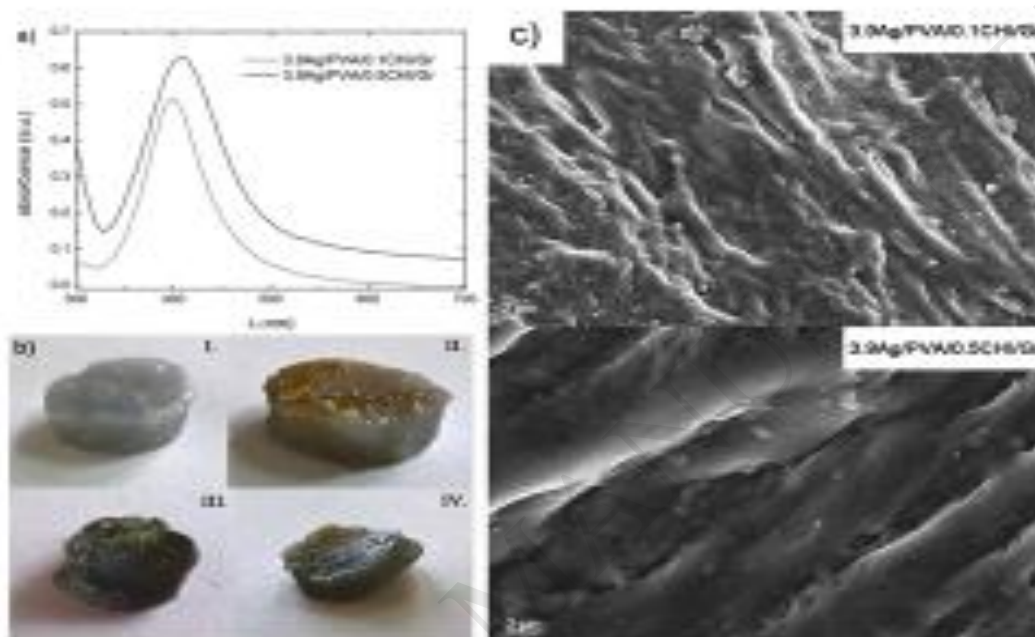
Fig. 2. Particle size distributions determined by DLS (a and e) and TEM micrographs (b-d and f-h) of AgNPs in (a-d) 3.9Ag/PVA/0.1CHI/Gr and (e-h) 3.9Ag/PVA/0.5CHI/Gr hydrogels.
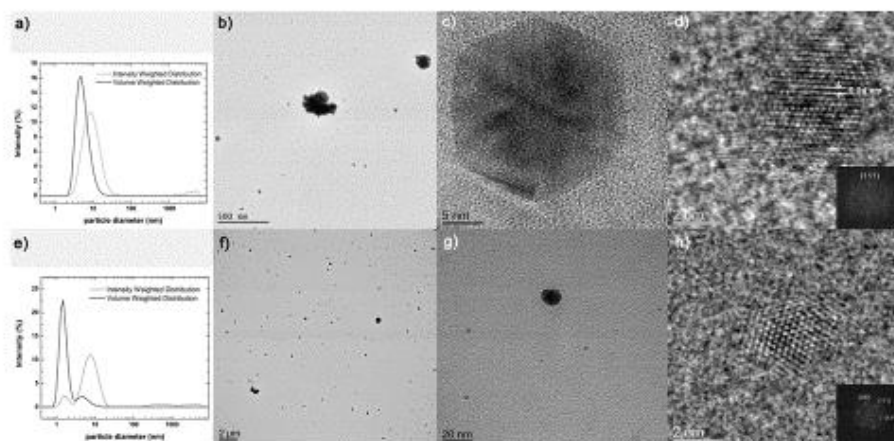
Fig.2

Fig. 3. FT-IR spectra of a) PVA/0.1CHI/Gr and 3.9Ag/PVA/0.1CHI/Gr and b) PVA/0.5CHI/Gr and
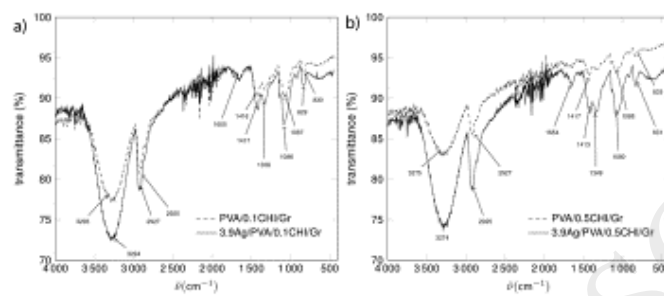
3.9Ag/PVA/0.5CHI/Gr.

Fig.3

Fig. 4. Stress-strain curves for PVA/0.1CHI, PVA/0.5CHI and PVA/0.5CHI/Gr.
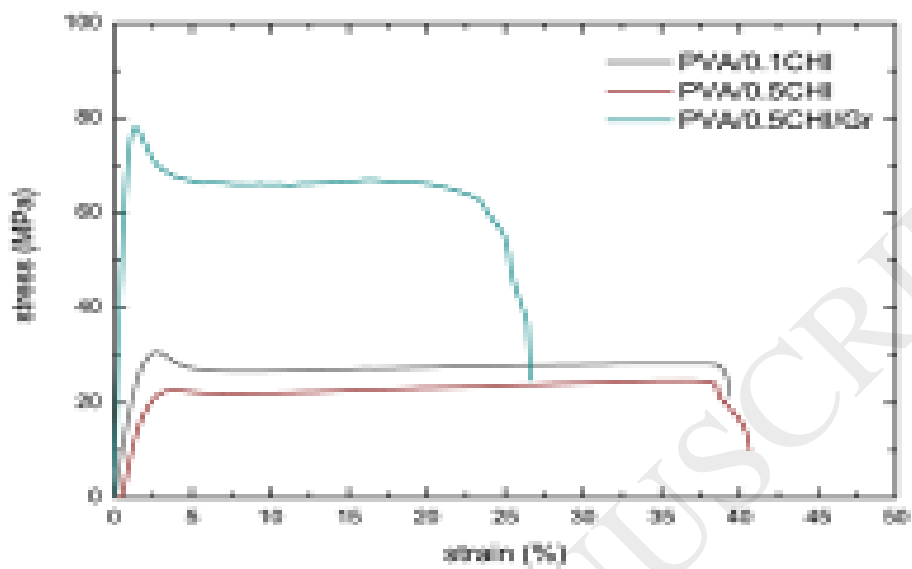
Fig. 5. DSC curves (exo up) of a) PVA/0.1CHI/Gr and 3.9Ag/PVA/0.1CHI/Gr, and b) PVA/0.5CHI/Gr and

3.9Ag/PVA/0.5CHI/Gr hydrogels.
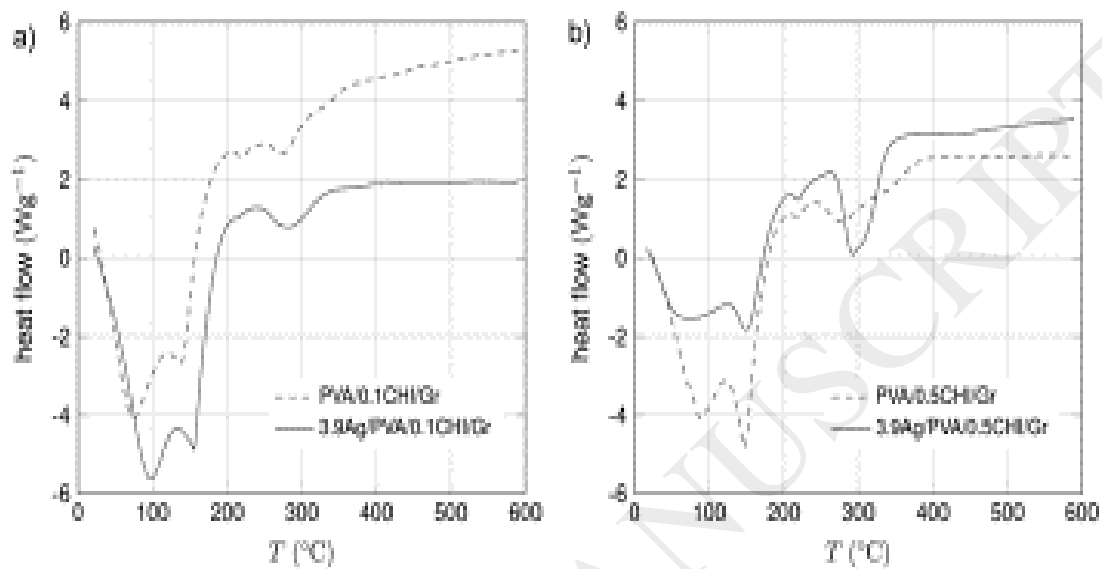
Fig. 6. Time dependence of swelling degree, q_t, in PB solution at 37 °C for a) PVA/0.1CHI/Gr and PVA/0.5CHI/Gr, b) 0.25Ag/PVA/0.1CHI/Gr, 0.25Ag/PVA/0.5CHI/Gr, 3.9Ag/PVA/0.1CHI/Gr and 3.9Ag/PVA/0.5CHI/Gr hydrogels.
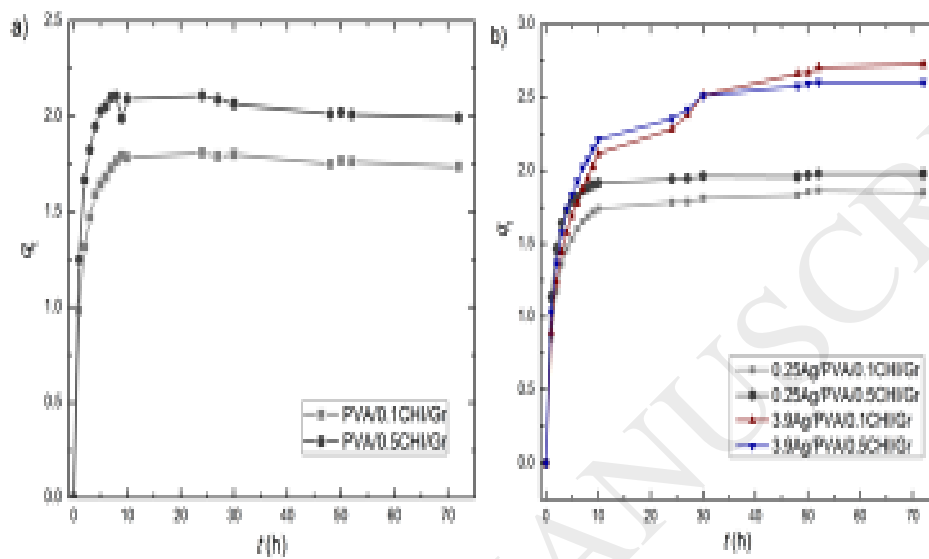
Fig. 7. Comparison of standard and modified early time approximations (ETA) for a) PVA/0.1CHI/Gr and b)
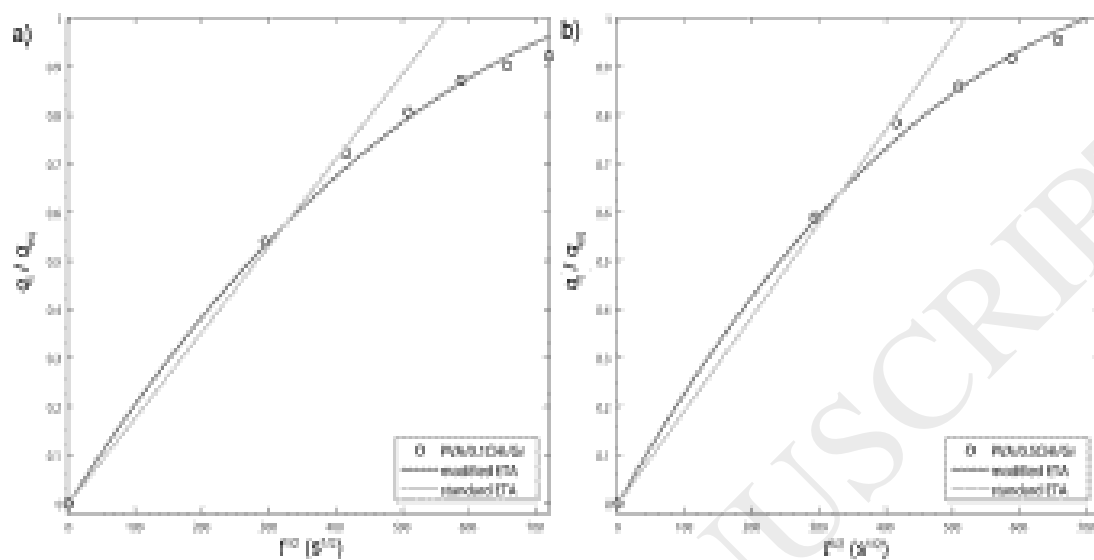
PVA/0.5CHI/Gr hydrogels.

Fig. 8. Early time (ETA), late time (LTA) and Etters approximations for a) PVA/0.1CHI/Gr and b)
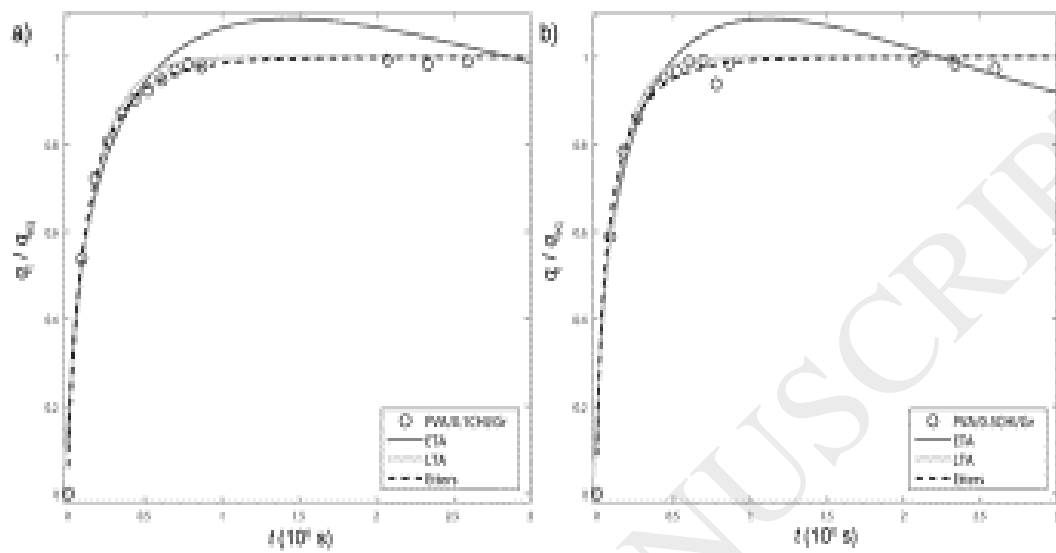
PVA/0.5CHI/Gr hydrogels.

Fig. 9. Etters approximations for a) 0.25Ag/PVA/0.1CHI/Gr and 0.25Ag/PVA/0.5CHI/Gr, b)

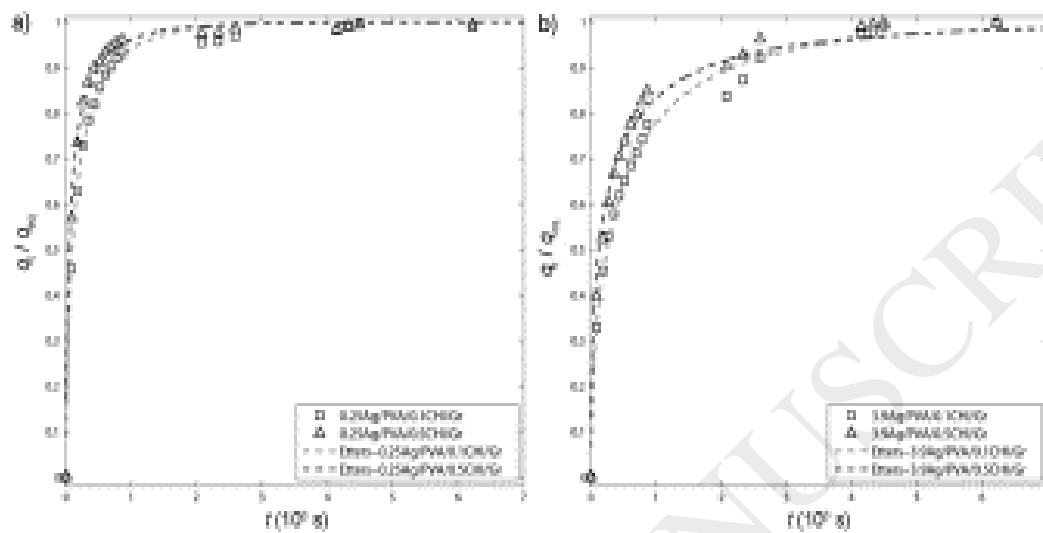3.9Ag/PVA/0.1CHI/Gr and 3.9Ag/PVA/0.5CHI/Gr hydrogels.

Fig. 10. a) Korsmeyer-Peppas and b) Makoid-Banakar models for experimental silver release profiles from 3.9Ag/PVA/0.1CHI/Gr and 3.9Ag/PVA/0.5CHI/Gr hydrogels.
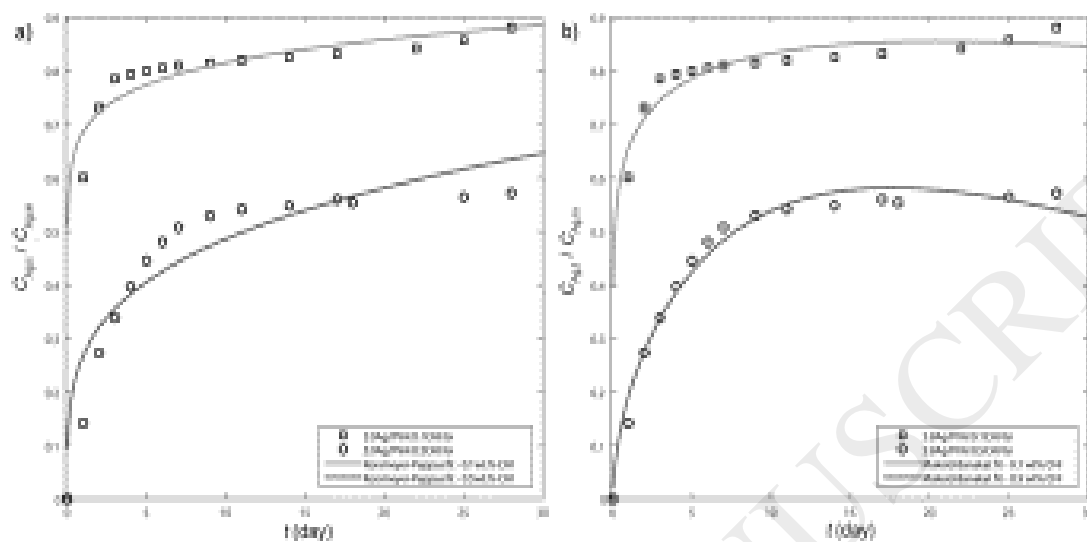
Fig. 11. Modified early time approximation (ETA) model for silver release profiles from 3.9Ag/PVA/0.1CHI/Gr and 3.9Ag/PVA/0.5CHI/Gr hydrogels.
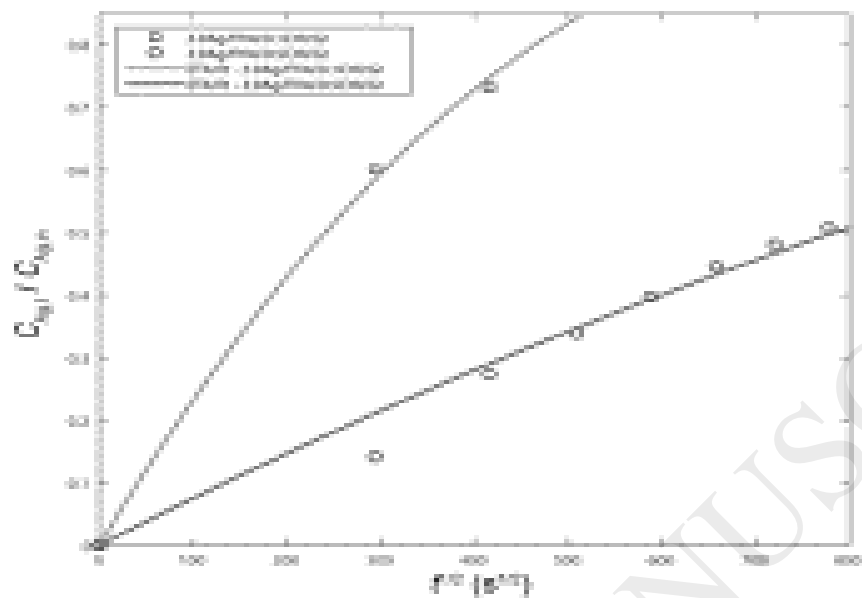
Fig. 12. Reduction of viable cells of a) *S. aureus* and b) *E. coli* before and after incubation in PB at 37 °C with PVA/0.1CHI/Gr, PVA/0.5CHI/Gr, 0.25Ag/PVA/0.1CHI/Gr and 0.25Ag/PVA/0.5CHI/Gr hydrogels.
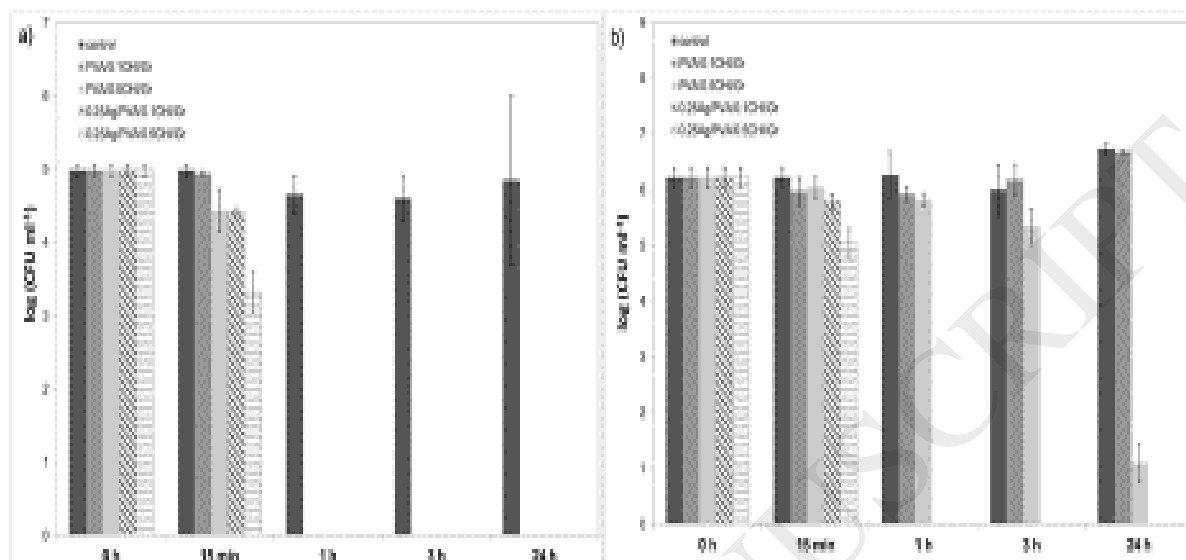
Table 1. Element content for PVA/0.1CHI/Gr, PVA/0.5CHI/Gr, 3.9Ag/PVA/0.1CHI/Gr and

3.9AgPVA/0.5CHI/Gr, determined by XPS

	Element content (at%)			
	PVA/0.1CHI/Gr	PVA/0.5CHI/Gr	3.9Ag/PVA/0.1CHI/Gr	3.9AgPVA/0.5CHI/Gr
C 1s	72.3	70.7	70.5	73.7
O 1s	27.3	28.4	27.4	23.3
N 1s	0.4	0.9	0.6	1.6
Ag 3d	–	–	1.5	1.4

Table 2. Mechanical properties of PVA/0.1CHI, PVA/0.5CHI and PVA/0.5CHI/Gr: σ_R – tensile yield strength, ε_R – yield elongation, E_J – Young's elasticity modulus, σ_U – ultimate strength, ε_R – ultimate elongation

	σ_R (MPa)	ε_R (%)	E_J (MPa)	σ_U (MPa)	ε_U (%)
PVA/0.1CHI	30.7	2.7	21.4	38.5	28.1
PVA/0.5CHI	22.6	3.8	14.0	24.4	38.0
PVA/0.5CHI/Gr	78.0	1.3	121.7	63.1	23.2

Table 3. Diffusion coefficients of the swelling medium, calculated from different sorption models, for

PVA/0.1CHI/Gr, PVA/0.5CHI/Gr, 0.25Ag/PVA/0.1CHI/Gr, 0.25Ag/PVA/0.5CHI/Gr,

3.9Ag/PVA/0.1CHI/Gr and 3.9Ag/PVA/0.5CHI/Gr hydrogels.

	D_E (10^{-8} cm^2 s^{-1}) (ETA)	D_L (10^{-8} cm^2 s^{-1}) (LTA)	D (10^{-8} cm^2 s^{-1}) (Etters)
PVA/0.1CHI/Gr	1.87	3.62	3.12
PVA/0.5CHI/Gr	2.40	4.65	3.53
0.25Ag/PVA/0.1CHI/Gr	1.41	2.39	1.74
0.25Ag/PVA/0.5CHI/Gr	2.22	3.70	2.36
3.9Ag/PVA/0.1CHI/Gr	0.610	1.04	0.940
3.9Ag/PVA/0.5CHI/Gr	0.876	1.50	0.983

Table 4. Fitting parameters obtained from Korsmeyer-Peppas, Makoid-Banakar and modified ETA models of silver release from 3.9Ag/PVA/0.1CHI/Gr and 3.9Ag/PVA/0.5CHI/Gr hydrogels

	Korsmeyer-Peppas model			Makoid-Banakar model				modified ETA model	
	k_{KP} (s^{-n})	n	R^2	C	n	k_{MB} (s^{-n})	R^2	D_{Ag} (10^{-8} cm^2 s^{-1})	R^2
3.9Ag/PVA/0.1CHI/Gr	0.686	0.075	0.981	0.0063	0.130	0.659	0.987	8.41	0.998
3.9Ag/PVA/0.5CHI/Gr	0.267	0.260	0.906	0.0330	0.581	0.197	0.983	0.723	0.974